CUKUROVA UNIVERSITY

INSTITUTE OF NATURAL AND APPLIED SCIENCES

MSc THESIS

Performance Optimization of a Snow Blowing Fan using Computational Fluid Dynamics

Gökhan KOCA

Mechanical Engineering Department

May, 2024

CUKUROVA UNIVERSITY

INSTITUTE OF NATURAL AND APPLIED SCIENCES

MSc THESIS APPROVAL

Performance Optimization of a Snow Blowing Fan using Computational Fluid Dynamics

---

Gökhan KOCA

Mechanical Engineering Department

This Master's Thesis was evaluated by the following Jury Members on 20/05/2024 and was approved by unanimity of votes.

Jury : Assoc. Prof. Dr. Göktürk Memduh ÖZKAN (Advisor) ……..

: Prof. Dr. Hüseyin AKILLI ……..

: Assoc. Prof. Dr. Tahir DURHASAN ……..

This Thesis was written in the Department of Mechanical Engineering, Institute of Natural and Applied Sciences.

Thesis Number:

Prof. Dr. Sadık DİNÇER
Director
Institute of Natural and Applied Sciences

Note: The usage of the presented specific declarations, tables, figures, and photographs either in this thesis or in any other reference without citation is subject to "The law of Arts and Intellectual Products" number of 5846 of Turkish Republic

CONTENTS

ABSTRACT I
ÖZ II
GENİŞLETİLMİŞ ÖZET III
ACKNOWLEDGEMENTS VI
LIST OF TABLES VII
LIST OF FIGURES VIII
SYMBOLS AND ABBREVIATIONS X
1. INTRODUCTION 1
1.1 General 1
1.2. Fans 3
1.3. Fan Types 4
1.3.1. Axial Fan 4
1.3.2. Centrifugal Fans 5
2. PRELIMINARY WORK 7
3. MATERIAL AND METHOD 11
3.1. Velocity Diagrams 11
3.2. Losses 13
3.3. Design Methodology 15
3.3.1. Impeller Design 15
3.3.2. Volute Design 25
3.3.3. Losses 27
3.3.4. Efficiencies 28
3.4. Fan Design 28
3.4.1. Calculations 29
3.5. Comparison of the Fan 33
3.5.1. Comparison of Impeller 33
3.5.2. Comparison of the Volute 37
3.5.3. Methodology 39
3.5.4 Validation Methodology of exact Geometry 46
4. RESULTS AND DISCUSSIONS 49
4.1 Tests and Validation 49
4.2. Optimization by CFD 53
4.2.1. Effect of blades on fan performance 54
4.2.2. Effect of blades angle on fan performance 59
5. CONCLUSIONS AND RECOMMENDATIONS 61

REFERENCES.....63
CURRICULUM VITAE.....65
APPENDICES.....67

CUKUROVA UNIVERSITY
INSTITUTE OF NATURAL AND APPLIED SCIENCES

MSc THESIS

Performance Optimization of a Snow Blowing Fan using Computational Fluid Dynamics

---

Gökhan KOCA

Advisor: Assoc. Prof. GÖKTÜRK MEMDUH ÖZKAN

Department of Mechanical Engineering

ABSTRACT

Centrifugal fans are frequently used in the industry to pressurize air. Backward-inclined blade centrifugal fans are used in many automotive and industrial applications, including snow sweeper vehicles. The main parts of the fan are the housing, blades, and motor. In centrifugal fans, the air enters perpendicular to the rotation axis of the blades, passes through the blades, and exits through the fan's housing outlet. After the movement of the fan blades, a pressure difference occurs between the inner and outer parts of the fan blades. Due to this pressure difference, air is drawn in from the fan inlet and directed to the outlet. This thesis investigates the effects of various parameters (such as the number of blades, impeller diameter, impeller width, impeller inlet, housing flow channel, and blade exit angles) on fan performance using a CFD approach. Parameters that positively influence flow and pressure will be examined from the literature. By determining appropriate values for the effective parameters and achieving the highest performance, the performance of the centrifugal fan used in snow plows and blowers for clearing runways at airports in winter conditions will be improved, dependency on external chemical fuel consumption will be reduced, and the resulting exhaust emission levels will be minimized. For this purpose, computational fluid dynamics (CFD) analysis were utilized. A three-dimensional solid model of the existing fan was created using the Catia program and adapted to the analysis environment (ANSYS-Fluent). According to the data evaluated by CFD, the blade structure, number of blades, housing structure, and power consumption corresponding to the highest fan performance were determined and reported.

Keywords: Centrifugal Fan, Computational Fluid Dynamics(CFD), Fan Performance, Optimization.

ÇUKUROVA ÜNİVERSİTESİ
FEN BİLİMLERİ ENSTİTÜSÜ

YÜKSEK LİSANS TEZİ

Hesaplamalı Akışkanlar Dinamiği Kullanılarak Kar Üfleme Aracının Fan Performans Optimizasyonu

Gökhan KOCA

Danışman: Doçent Dr. Göktürk Memduh ÖZKAN

Makine Mühendisliği Bölümü

ÖZ

Santrifüj fanlar endüstride havayı basınçlandırmak amacıyla sıklıkla kullanılmaktadır. Geriye eğik kanatlı santrifüj fanlar, Kar Temizleme Süpürgesi araçları da dahil olmak üzere birçok otomotiv ve endüstriyel alanlarda kullanılmaktadır. Fanın temel parçaları salyangoz, kanatlar ve motordur. Santrifüj fanlarda kanatların dönme eksenine dik olarak giren hava, kanatların arasından geçtikten sonra fanı salyangoz çıkışından terk eder. Fan kanatlarının hareketinden sonra fan kanatlarının iç ve dış kısımları arasında basınç farkı oluşur. Bu basınç farkından dolayı fan girişinden hava emilir ve çıkışa yönlendirilir. Bu tezin amacı çeşitli parametrelerin (kanat sayısı, çark çapı, çark genişliği, çark girişi, salyangoz akış kanalı, kanat çıkış açıları gibi) fan performansı üzerindeki etkilerini HAD yaklaşımıyla araştırmaktır. Akış ve basıncı olumlu yönde etkileyen parametreler literatürden incelenmiştir. Etkin parametrelerde uygun değerlerin belirlenerek en yüksek performansın elde edilmesiyle havalimanlarının kış şartlarında pistteki karı temizlemek için kullanılan kar küreme ve üfleyicideki santrifüj fanın performansının arttırılması, dışarıya bağımlı olan kimyasal yakıt tüketiminin azaltılması ve oluşan egzoz emisyon düzeyinin en aza indirilmesi amaçlanmaktadır. Bu amaçla hesaplamalı akışkanlar dinamiği (HAD) analizinden yararlanılmıştır. Mevcut fanın üç boyutlu katı modeli Catia programıyla oluşturularak analiz ortamına (ANSYS-Fluent) uyarlanmıştır. HAD tarafından değerlendirilen verilere göre en yüksek fan performansına karşılık gelen kanat yapısı, kanat sayısı, salyangoz yapısı ve güç tüketimi ortaya çıkarılmış ve raporlanmıştır.

Anahtar Kelimeler: Santrifüj Fan, Hesaplamalı Akışkanlar Dinamiği (HAD), Fan Performansı, Optimizasyon.

GENİŞLETİLMİŞ ÖZET

Günümüzde, dünyada 8 milyar insan yaşamakta ve her insanın günlük ortalama 1,03 kg atık bıraktığı varsayılmaktadır. Ayrıca hızlı kentleşme, teknolojinin hızla ilerlemesi doğal kaynaklarımızı tehdit etmekte ve çevre kirliliğine neden olmaktadır. Fakat çevre hakkının, en temel insan haklarından biri olduğu da bilinmektedir. Bu nedenle çevrenin korunmasına yönelik yapılacak her aktivite ve atılacak her adım insanlık yararına yapılmış olacaktır. Sağlıklı bir toplum oluşturulmasının yolu, çevre sorunlarının çözülmesiyle mümkün olacağı günümüzde kabul görmüş bir gerçektir.

Çevre kirliliğine neden olan atıkların, atık yönetim sistemi ile bertaraf edilmesi konusu önemini sürekli arttırmaktadır. Atık yönetimi konusunda kamu kurumlarının üzerine düşen görevler bulunmaktadır. Kamu kurumları, özellikle temizlik konusunda çeşitli bölümler ile atık yönetimi konularında uzmanlaşarak görevlerini yerine getirmektedirler. Bu konu özelinde, belediyeler ve havalimanı işletmeciliğini yapan kurumlar, çevre temizliğinde görevlendirmek üzere, taşıyıcı bir kamyon üzerine monte edilmiş yol ve pist süpürgesi araçları ile kar küreme, üfleme araçları temin etmektedirler. Bu araçlar ile kurumlar, çevre temizliği konusunda, kısa sürelerde büyük alanları temizlemede başarı sağlamaktadırlar. Bu başarının arkasında, hizmet araçlarında kullanılan ve mühendislik hesapları ile sürekli geliştirilen merkezkaç fanları yer almaktadır.

Bu çalışmanın amacı, hava alanlarının, sokak aralarının, pazar yerlerinin, özel işletmelerin temizlenmesinde aktif rol alan vakumlu yol ve pist süpürgesi araçlarında ve kar küreme, üfleme araçlarında kullanılan merkezkaç fanının performansını artırmaktır. Merkezkaç fanına ait kanat sayılarının, kanat açılarının, kanat fiziki yapılarının (çark genişliği, çark çapı, vs.), salyangoz ve sıvama yapılarının incelenerek güç tüketimini azaltmak, aynı güç tüketiminde daha yüksek debi elde edebilmek ve verimini artırmak hedeflenmiştir. Dışa bağlı olan fosil yakıt ihtiyacını düşürmek ve çevre kirliliğini azaltarak doğayı korumaya yönelik çalışma amaçlanmıştır.

Hava ve benzeri gazları basınçlandırarak belirli bir akış içerisinde hareket etmesini sağlayan turbo makinelere fan denilmektedir. Eksenel fan, merkezkaç fan, çatı tipi fanlar, çapraz akışlı blowerlar, vortex veya rejenatif fan çeşitleri mevcuttur. Gövde, çark, kanat bir fanın ana donanımlarıdır. Bina havalandırma sistemleri, demir çelik, cam, çimento, ahşap sanayi, karayolu, demiryolu tünel havalandırması, rüzgâr tüneli, taşımacılık, otomotiv, endüstriyel havalandırma gibi sektörlerde kullanım alanına sahiptir. Havaalanlarında pist, apron, taksi yollarının temizliğinde, belediyelerde bulvarların, sokak aralarının, kara yollarının temizliğinde, pazar yerlerinde, özel işletmelerin iç temizliğinde fan ile negatif basınç yaratarak hava aracılığıyla temizlik sağlamaktadır. Fanların tahrikinde endüstriyel alanda genel olarak elektrik motoru kullanılmaktadır. Mobil sektörde ise kar küreme üfleme, yol süpürgesi gibi alanlarda endüstriyel tip dizel motor aracılığıyla tahrik tercih edilmektedir. Dizel motor fosil enerjiyi mekanik enerjiye çevirmektedir. Mekanik enerji direkt olarak mil aracılığıyla fana bağlanarak çarkın dönmesinin sağlanması bir yöntemdir. Diğer bir

yöntem ise dizel motor volanına hidrolik pompa monte edilerek mekanik enerjinin hidrolik enerjiye dönüşümü sağlanmaktadır. Hidrolik pompa dizel motordan kazandığı mekanik enerji sayesinde hidrolik yağı sıkıştırarak basınçlandırmakta ve mekanik enerjiyi hidrolik enerjisine çevirmektedir. Basınçlandırılan hidrolik yağ, hidrolik hortum ve bağlantı elemanları aracılığı ile fan çarkına akuple olan hidrolik motora aktarımı sağlanmaktadır. Fan çarkına farklı yataklama tipleri ile bağlı hidrolik motor pompadan temin etmiş olduğu hidrolik gücü mekanik güce çevirmektedir. Çarka böylece mekanik güç aktarılmakta ve çarkın dönmesi sağlanmaktadır. Hidrolik yöntem ile tahrikin mekanik yöntem tahrikinden bir takım avantajları mevcuttur. Bunların en temel olanı istenilen hidrolik deplasman hacminde kontrol sağlanabilmesidir. Operatör kontrolünde çevre kirlilik durumuna bağlı olarak farklı dönüş devirlerinde kullanım olanağı sağlamaktadır. Bu da ihtiyaç fazlası enerji tüketiminin önüne geçmekte ve enerji tasarrufu getirisinde bulunmaktadır.

Çalışma kapsamında mevcutta yer alan; tedarik edilmiş Kar Küreme ve Üfleme aracında kullanılan merkezkaç fanı inceleme altına alınmıştır. Örnek fan, endüstriyel tip dizel motor volanına bağlı dişli kutusu aracılığıyla güç aktarımı sağlanmakta ve dişli kutusuna montajlanmış kapalı çevrim hidrolik pompanın oluşturduğu basınçlı hidrolik yağ aracılığıyla merkezkaç fanını çevirmekte kullanılan hidrolik motorun tahrikiyle çalışmaktadır. Santrifüj tip geriye yatık Z=13 kanatlı, S355J2 kalite siyah sacdan imal edilmiş, çıkışında akışı basınçlandırmak ve akış hızını artırmak için üfleme bacası bulunan bir fandır. Öncelik olarak fan çıkışında bulunan üfleme kanalı demonte edilmiştir. Üfleme kanalı yerine test yapılabilmesi üfleme bacasının çıkış alanına istinaden uygun akış kanalı oluşturularak üfleme bacasına bağlanmıştır. Kanal üzerinde akışın yüksek türbülansa sahip olmasından dolayı kanal kesiti üzerinde farklı noktalardan pitot tüpü ile her bir noktadan ölçüm alınarak kanalın ortalama hızı belirlenmiştir. Dijital bir takograf aracılığıyla; sensör ile kullanıcı arayüzüne aktarılan dizel motorun ve fan devirlerini doğrulamak adına ölçümler yapılmış olup değerler eşleştirilmiştir. Manometre aracılığı ile kapalı çevrim hidrolik sisteminin basınçları ölçülmüştür. Ölçümler neticesinde kayıpların da göz önünde bulundurulmasıyla fanın harcamakta olduğu güç hesaplanmıştır. Dizel motorun harcadığı güce istinaden tüketmekte olduğu yakıt, üretici performans grafikleri üzerinden çalışma devrinde üretilen güç ve yakıt eğrisi kullanılarak belirlenmiştir. Daha sonra geriye yatık kanatlı merkezkaç fan demonte edilerek ürünün teknik çizimleriyle kıyaslaması gerçekleştirilmiştir. İki boyutlu (2D) teknik çizim kontrolü ile ürün doğrulanmış ve üç boyutlu (3D) olarak modellenerek Hesaplamalı Akışkanlar Dinamiği analizlerini gerçekleştirmek üzere ANSYS yazılımı içerisine adapte edilmiştir.

Akışa etkisi olmayan ve analiz programının performansını düşürecek, çözüm sürecini uzatacak potansiyelde olan parça ve montaj grupları çıkartılarak akış hacmi oluşturulmuştur. Daha sonra program içerisinde yer alan ve kaynaklarda kabul görmüş olan kalite değerleri elde edilene kadar ağ elemanlarının düzenlemesi gerçekleştirilmiştir. Sınır şartları tanımlanarak isimlendirilmiş ve oluşturulan akış hacminin çözümü için analiz ortam koşulları tanımlaması, çözüm algoritmaları ve kullanılacak yöntemler seçilmiştir.

Teorik hesaplamalar ve sayısal analiz sonuçları, test verileri ile kıyaslanmış olup, makul seviyede veriler elde edilmiştir. Buna göre, merkezkaç fan üzerinde yapılacak fiziki değişikliklerin aynı analiz çözüm koşullarında kabul edilebilir sonuçlar vereceğini kanıtlamıştır. Bu bağlamda analitik hesaplama verileri ile mevcut fan geometrisi değiştirilmiştir. Analiz ortamında analitik hesaplanan geometri üzerinde çalışma gerçekleştirilmiştir. Eniyileme kapsamında fiili olarak salyangoz yapısının değiştirilmesi, tüm sistemi etkilemesinden dolayı analitik hesaplamada elde edilen çark genişliği ile salyangoz ilişkisine göre hesap revize edilerek elde edilen çark genişliği ile analiz çalışılmıştır. Elde edilen sonuçlar verimin artırmış olmasından dolayı sonraki aşamaya w: 113mm çark genişliği ile devam edilmiştir. Daha sonra Z= 9 ile Z= 17 kanat sayısı arasında analizler gerçekleştirilmiştir. Analiz sonuçlarına istinaden Z=15 kanatlı fan çarkında karar kılınmıştır ve sonraki aşamaya Z=15 kanatlı geometri ile geçiş yapılmıştır. Nihayetinde hesaplama çizelgesi kullanılarak farklı çark çapları üzerinde çalışma gerçekleştirilmiştir. Yapılan çalışmalar neticesinde salyangoz yapıdan çarka doğru gerçekleşen akış geçişinde ters akış ve düşük basıncın tespit edilmesi ile çark sıvama geometrisi ve salyangoz çark arası akış kanalı üzerinde çalışma gerçekleştirilmiştir. Gerçekleştirilen bu aşamada hesaplama verilerine göre çarkın giriş geometrisine ve salyangoz yönlendirme kanalına kavis verilmiş, bu iki bölgenin birbirleri ile olan yükseklik ve iç içe girme mesafeleri revize edilerek analiz ortamında olumlu sonuçlar elde edilmiştir. Son olarak kanat açısı değerleri göz önünde bulundurularak yenileme çalışmaları gerçekleştirilmiştir.

Yapılan çalışmaların nihayetinde, kanat sayısının Z=15, çark çapının ϕ840mm, çark genişliğinin w=113mm, çark sıvama yarıçapının R= 90mm ve salyangozdan çarka akışı yönlendiren geometri yarıçapının R= 103mm olduğu, kanat çıkış açısının mevcut üründe olduğu gibi β_2: 45^0 olduğu fiziksel yapılı merkezkaç fanının en verimli çalışma noktası olarak belirlenmiştir.

ACKNOWLEDGEMENTS

First of all, I would like to thank my advisor, Associate Professor Dr. Göktürk Memduh ÖZKAN, for his support and guidance throughout my thesis process.

I would also like to thank my family and especially my wife Betül KOCA for their devotion and moral support. In addition, I would like to thank the management of Koluman Otomotiv Endüstri A.Ş., my manager Erhan BİÇER and my colleagues, especially Hüseyin Atakan BAYTAŞ and Mehmet Ali KURGUN, who attach importance to and support my academic studies.

LIST OF TABLES

Table 1.1. World Energy Demand Development 2
Table 3.1. Designed Church fan impeller drawing schedule 32
Table 3.2. Comparison of impellers 33
Table 3.3. Redesigned Church fan impeller drawing schedule 36
Table 3.4. Comparison of redesigned impellers 37
Table 3.5. Skewness mesh metrics spectrum 42
Table 3.6. Skewness value of the tested fan 43
Table 3.7. Orthogonal Quality mesh metrics spectrum 43
Table 3.8. Orthogonal quality values of modeled tested fan 43
Table 3.9. Independent geometrical parameters 45
Table 3.10. Dependent and constant geometrical parameters 45
Table 4.1. Result differences of hydraulic hoses 51
Table 4.2. Skewness value of the KOE fan 51
Table 4.3. Orthogonal Quality of KOE fan 51
Table 4.4. Comparison of results between tested fan and analyzed tested fan 53
Table 4.5. Comparison of the analyzed KOE fan and the impeller designed according to Church 54
Table 4.6. Comparison the width of Impeller by CFD results 56

LIST OF FIGURES

Figure 1.1. 2018 Distribution of primary energy supply development by sources 2
Figure 1.2. 2018 Sectoral breakdown of primary energy consumption 3
Figure 1.3. Axial fan..... 5
Figure 1.4. Centrifugal Fan (a) Rotor, (b) Volute 5
Figure 1.5. Six blade shapes commonly used in centrifugal fans with maximum efficiency 5
Figure 2.1. Q-H curves with losses 8
Figure 3.1. Comparison of losses in different design methods with experimental results 11
Figure 3.2. Relative and absolute velocities..... 11
Figure 3.3. Inlet and outlet speed diagrams of single suction backward inclined vane impeller .. 12
Figure 3.4. Impeller sections 12
Figure 3.5. Rotational Flow, Straight Flow and its Combination 14
Figure 3.6. Inlet and Outlet Velocity Diagrams with Circulatory Flow Correction 14
Figure 3.7. Volute Cross Section..... 25
Figure 3.8. Scroll Casing Design by 4 Point Method..... 25
Figure 3.9. Drawing of impeller according to Church design..... 32
Figure 3.10. Drawing of the tested fan impeller 33
Figure 3.11. Tested fan with blowing unit..... 35
Figure 3.12. Tested fan without blowing unit..... 35
Figure 3.13. Church redesigned impeller..... 36
Figure 3.14. KOE snow ploughing fan 38
Figure 3.15. Designed volute 4-point method..... 38
Figure 3.16. Volume flow of tested fan impeller..... 40
Figure 3.17. Volume flow of tested fan 40
Figure 3.18. Volume flow of tested fan 41
Figure 3.19. Meshing model 41
Figure 3.20. Meshing model of tested fan..... 42
Figure 3.21. Skewness of the tested fan..... 42
Figure 3.22. Orthogonal Quality of tested fan 43
Figure 3.23. Geometrical parameters..... 44
Figure 3.24. Exact geometry 45
Figure 3.25. Gear reducer..... 46
Figure 3.26. System schematic..... 46
Figure 3.27. Closed loop hydraulic circuit..... 47
Figure 3.28. Engine performance curves (MTU, OM470) 47

Figure 4.1. Measurement with digital tachometer 49
Figure 4.2. Measurement of air velocity…….. 49
Figure 4.3. Meshing of KOE fan 51
Figure 4.4. Pressure contour of tested fan 52
Figure 4.5. Velocity contour of tested fan 53
Figure 4.6. Pressure contour of the tested fan impeller 53
Figure 4.7. Pressure contour of Church design impeller 54
Figure 4.8.Velocity contour of Church design impeller..... 54
Figure 4.9. Pressure contour of the 57mm wide Impeller 55
Figure 4.10. Pressure contour of the 113mm wide Impeller 55
Figure 4.11. Velocity contour of the 57mm wide Impeller..... 55
Figure 4.12. Velocity contour of the 113mm wide Impeller..... 55
Figure 4.13. Relationship between the number of blades with pressure differences and efficiency 56
Figure 4.14. Pressure contour of the 770mm diameter Impeller..... 57
Figure 4.15. Pressure contour of the 840 mm diameter Impeller..... 57
Figure 4.16. Velocity contour of the 770mm diameter Impeller 58
Figure 4.17. Velocity contour of the 840mm diameter Impeller 57
Figure 4.18. Geometry of Impeller redesigned Shroud Radius..... 58
Figure 4.19. Pressure Contour of redesigned Shroud Radius 58
Figure 4. 20. Velocity Contour of redesigned Shroud Radius 58
Figure 4.21. Redesigned geometry of the nozzle 59
Figure 4. 22. Pressure Contour of the redesigned nozzle..... 59
Figure 4.23. Velocity contour of the redesigned nozzle 59

SYMBOLS AND ABBREVIATIONS

A_1	:	Impeller blade area Assumption: Leakage loss %3
A_2	:	Impeller outlet area
A_v	:	Exit volute area
b_1	:	Blade inlet width
b_2	:	Blade exit height
b_3	:	Width of volute casing
c_p	:	Specific heat at constant pressure
c_v	:	Specific heat at constant volume
D_1	:	Impeller blade inlet diameter
D_2	:	Impeller outside diameter
D_{duct}	:	Diameter of duct
D_{inlet}	:	Impeller inlet diameter
d_{hose}	:	Diameter of hydraulic hose
$dP_{impeller}$	:	Impeller pressure Lose
$dP_{suction}$	:	Suction pressure lose
f	:	Material friction constant
FOS	:	Factor of safety
g	:	Gravity force
G	:	Ideal shaft power
H_v	:	Height of volute
H	:	Head
H_{ad}	:	Adiabatic Head
$H_{eff.}$	:	Effective head
$H_{theo.}$	:	Theoretical head
i_{gb}	:	Transmission coefficient
K'	:	Coefficient for friction and turbulence
k_i	:	Suction pressure loss coefficient
k_{ii}	:	Impeller pressure loss coefficient
k_{iii}	:	Losing constant
KOE	:	Koluman Automotive Industry
l_c	:	Clearance
l_o	:	Overlap
$\dot{m}$	:	Mass flow rate
N	:	Rotation of impeller
N_{pump}	:	Hydraulic pump rotation
N_{engine}	:	Diesel engine rotation
$N_{hyd.motor}$	:	Hydraulic motor rotation
P_2	:	Outlet pressure of impeller
P_{atm}	:	Atmospheric Pressure
P_{atm}	:	Atmospheric Pressure

P_{df} : Power loss due to disc friction
P_{inlet} : Inlet pressure
P_{static} : Static Pressure
Q : Flow rate
Q_{inlet} : Flow rate inlet
Q_L : Leakage lose
Q_{outlet} : Volumetric flow rate at the outlet
q_{pump} : Hydraulic pump displacement
$q_{hydr.motor}$: Hydraulic motor displacement
R : Ideal gas constant
R_2 : Volute base circle/inlet radius
R_3 : Radius of volute at angle 360º
R_t : Radius of volute tongue
r_n : Nozzle Radius
r_s : Shroud radius
t : Blade thickness
T_2 : Outlet temperature
T_{atm} : Temperature of air at atmospheric pressure in C
T_{df} : Disk friction lose
T_{inlet} : Temperature inlet
u_1 : The circumferential tangential velocity at the blade
u_2 : Tangential velocity at the outlet of impeller
v_1 : Impeller inlet relative velocity
v_2 : Absolute blade velocity
V_3 : Outlet velocity of Volute
V_{duct} : Velocity of inlet duct (assuming)
V_{inlet} : Velocity of inlet
$V_{hydraulic}$: Volume of Hydraulic Pump
V_{r1} : Blade radial inlet velocity
V_{r2} : Radial outlet velocity
V_{u2} : Tangent outlet velocity vector
V'_{u2} : Swirl velocity
W_z : Slip factor
W_{u2} : Impeller inlet relative velocity with slip
W'_2 : Outlet relative velocity with slip
W : Power
Z : Blade number
β_1 : Assumption: increase 3% for contraction of stream at inlet
β_2 : Blade outlet angle
$\acute{\varepsilon}_1$: Blade inlet area thickness correction factor
$\acute{\varepsilon}_2$: Outlet blade thickness factor
ε_p : Pressure ratio impeller

$\varepsilon_{P\ imp}$: Impeller outlet pressure is based upon effective head

$\varepsilon_{p\ inlet}$: Pressure ratio

θ_t : Volute tongue angle

ρ_2 : impeller outlet density

$\rho_{\ air}$: Density of air

$\rho_{\ atm}$: Density of air at atmospheric pressure

$\rho_{\ inlet}$: density of air at inlet

V'_2 : Absolute Velocity

α'_2 : Air angle

$\eta_{\ hydr.}$: Hydraulic efficiency

$\eta_{\ vol}$: Volumetric efficiency

$\eta_{\ total}$: Total efficiency

$\eta_{\ hydr.motor}$: Mechanical efficiency for hydraulic motor

$\eta_{\ hydr.pump}$: Volumetric efficiency for hydraulic pump

$dP_{\ Volute}$: Volute loss

ω : Angular velocity of impeller

1. INTRODUCTION

1.1 General

Energy, which lies at the heart of environmental problems, is a key element of the life cycle and development. is one of the basic elements. Industry, transport and buildings are the main consumers of energy. (use) areas. Today, about 90 per cent of energy is of fossil origin. fuels (coal, oil, natural gas). Very important technological Unless there is a breakthrough, this situation will continue in the near future. Fossil fuels emissions resulting from combustion (CO_2, CO, SO_2, NOx) in the atmosphere The greenhouse effect occurs with the accumulation and the ecological balance of the earth is disrupted. In other words, emissions and other wastes increase, natural resources decreases, air and water pollution increases. In addition, due to the increasing demand, the known reserves of fossil fuels are decreasing and can meet less and less of the increasing demand. This situation causes the prices of fuels to increase and/or fluctuate. For all these reasons, there are intensive efforts to use energy efficiently and to use renewable energy sources more in order to reduce the consumption of fossil-based fuels all over the world, but it is progressing slowly.

Policies, technologies and practices that enable the continuous supply of the required energy at optimum financial, environmental and social costs are defined as energy sustainability. In other words, it is necessary to reduce the negative impacts of energy production and utilization on the environment and to develop environmentally friendly strategies and these strategies should also be economical. Protection of resources (energy, water, etc.), environment and economy constitute the three main components of sustainable development.

Growth in global energy consumption decreased in 2022, but remained above the average between 2010 and 2019. While growth decreased in the world's strongest economies, an increase was observed in countries with strong economic growth. On the other hand, primary energy consumption in Europe declined as industrial and residential consumers were incentivized to reduce their energy demand due to rising energy costs and mild temperatures caused by the Russian-Ukrainian war. Primary energy sources meeting the world energy demand and CO_2 emission amounts are given in Table 1.1. (Enerdata, 07.01.2024)

Table 1.1. World Energy Demand Development (Enerdata, 07.01.2024)

	Global World				
				Politics	
	2000	**2017**	**2018**	**2025**	**2040**
Coal	2,217	3,718	3,772	4,165	5,045
Fuel oil	3,519	4,607	4,662	4,815	5,477
Natural gas	2,158	3,142	3,309	3,514	4,682
Nuclear	585	597	611	839	997
Hydroelectric	617	920	949	409	513
Other renewable		490	561	1,948	2,584
TOTAL	9,095	13,475	13,865	15,690	19,298
Fossil Fuel %	87	85	85	80	79
Fuel oil %	39	34	34	31	28
CO_2 emission Million tonnes CO_3	23,668	33,243	33,891	35,000	43,000

Primary energy supply in Turkey was as shown in Figure 1.1. 143.7 million the tonne of oil equivalent (TOE) in 2018. The share of natural gas in primary energy demand was 28.7%, coal 28.4%, oil 29.2%, hydraulic energy 3.6% and non-hydraulic renewable energy sources 12.2% (Aydın and et al., 2020).

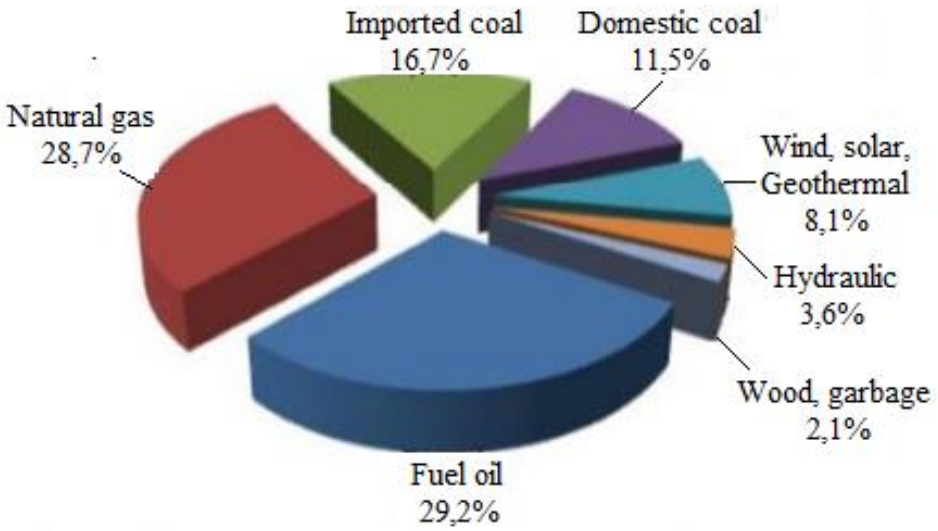


Figure 1.1. 2018 Distribution of primary energy supply development by sources

When the distribution of our primary energy supply by sectors is analyzed, it is seen that 25% is used in industry, 24% in housing and service sector, 23% in transport, 23% in conversion, 4% in non-energy use and 3% in agriculture and livestock sector (see Figure 1.2.). It is estimated that the foreign dependency ratio, which is currently 93% for oil and 99% for natural gas, will continue at approximately the same levels in the coming years. (Aydın and et al., 2020).

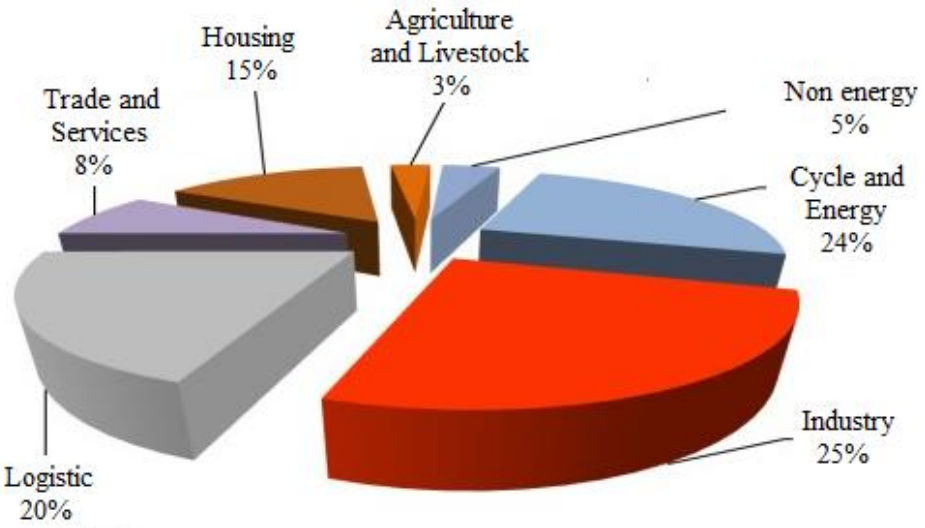


Figure 1.2. 2018 Sectoral breakdown of primary energy consumption

1.2. Fans

According to AMCA Standard 99-0066, a fan is a driven impeller for conveying air or gases is defined as a device that is energized by. A fan consists of a rotating arrangement of vanes or blades, generally made of wood, plastic, or metal, which act on the air. The rotating assembly of blades and hub is known as an impeller, rotor, or runner. Usually, it is contained within some form of housing, or case (Encyclopædia Wikipedia. Retrieved 07.01.2023). It is used in sectors such as building ventilation systems, iron and steel, glass, cement, wood industry, highway, railway tunnel ventilation, wind tunnel, transport, automotive, industrial ventilation. It provides cleaning through air by creating negative pressure with the fan in the cleaning of runways, aprons, taxiways at airports, cleaning of boulevards, streets, roads in municipalities, market places, interior cleaning of private enterprises.

Electric motor is generally used in the industrial field in the drive of the fans. In the mobile sector, industrial type diesel engine drive is preferred in areas such as snow ploughing blowing, road sweeper. Diesel engine converts fossil energy into mechanical energy. One method is to connect the mechanical energy directly to the fan through the shaft and ensure the rotation of the impeller. Another method is to install a hydraulic pump on the diesel engine flywheel to convert mechanical energy into hydraulic energy. The hydraulic pump pressurizes the hydraulic oil by compressing it thanks to the mechanical energy gained from the diesel engine and converts the mechanical energy into hydraulic energy. The pressurized hydraulic oil is transferred to the hydraulic motor coupled to the fan wheel through hydraulic hose and fittings. The hydraulic motor connected to the fan wheel

with different bearing types converts the hydraulic power obtained from the pump into mechanical power. Thus, mechanical power is transferred to the impeller and the impeller rotates.

According to the data of the Ministry of Energy and Natural Resources, Turkey's electrical energy consumption in 2022 decreased by 0.5% compared to the previous year to 331.1 TWh and electricity generation decreased by 1.9% compared to the previous year to 328.3 TWh. (T.C. Enerji ve Tabii Kaynaklar Bakanlığı 08.01.2023)

Efficient use of energy in fans and fan systems can be achieved by optimizing fan selection, manufacturing and operation processes. Because fans consume hundreds of times more energy than their initial investment costs during their lifetime.

Therefore, manufacturers should take into account the price and the energy it will consume when purchasing a fan. This means that the best fan for a business is not the fan with the lowest initial investment cost. When purchasing a fan and the system in which the fan will be operated.

When designing the project, great attention should be paid to such issues. What should be done here is to select the fans on a lifetime cost basis, i.e. when determining the initial investment costs (Bulgurcu, 2015).

1.3. Fan Types

Fans can be classified in different ways. (Bleier, 1985)

- Axial fans
- Centrifugal fans,
- Axial-centrifugal fans,
- Roof type fans,
- Cross flow blowers,
- Vortex or regenerative fans.

The most commonly used of these, Axial and Centrifugal Fans, detailed below explained.

1.3.1. Axial Fan

Without changing the direction of the fluid in the same axis with the fan wheel, In other words, axial fans, in which the flow of the fluid at the impeller outlet is parallel to the shaft axis, are generally preferred in high flow and low pressure applications. Noise levels are high. They have different body structures according to the place of use. Duct, wall, roof, etc. Although there are many areas of use, they are mostly used as exhaust fans.



Figure 1.3. Axial fan

1.3.2. Centrifugal Fans

Centrifugal (radial/centrifugal) fans are fans in which the fluid exits the impeller perpendicular to the shaft axis, i.e. in the radial direction. Used to overcome high flow resistances. Generally preferred in high pressure and low flow applications.

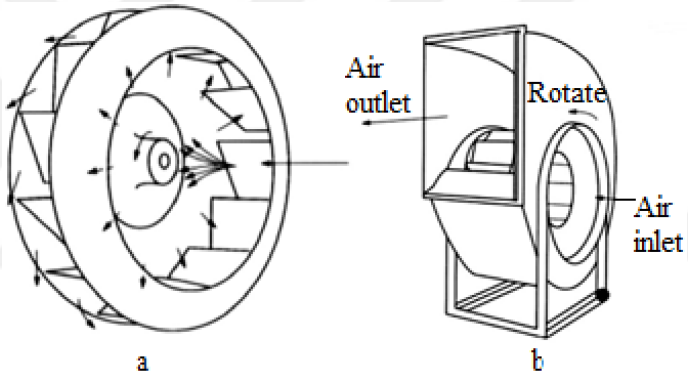


Figure 1.4. Centrifugal Fan (a) Rotor, (b) Volute

6 different types of centrifugal fans can be in different blade shapes, each of which has advantages and disadvantages depending on industrial applications. AF (airfoil), BC (backward-curved), BI (backward-inclined), RT (radial-tip), FC (forward-curved) and RB (radial blade) (Bleier, 1985).



Figure 1.5. Six blade shapes commonly used in centrifugal fans with maximum efficiency (Bleier, 1985)

2. PRELIMINARY WORK

Church (1947) is one of the first to compile the design method of pumps and blowers. In pumps or fans, the Reynolds number of the flow always exceeds a certain critical number, that is, the flow is turbulent; therefore, the flow said that there was a serious pressure loss. It included the compressibility effect, pressure ratio and energy transfer in its design. In addition, it has taken into account the variability of the density of the fluid due to temperature and pressure differences in certain parts of the fan. He suggested that this caused the volumetric flow rates to be constantly changed. This volumetric flow rate changes have been taken into account when determining the cross-sections of fluid passages. In the total head formula, he defined a "total pressure coefficient, K" for the pressure loss due to turbulence and friction in the impeller and found that it is between 0.5 and 0.65 through the experiments.

Later, researchers such as Bruno (1972), and Osborne (1977) developed studies on Church's methods. Eck Bruno (Bruno, 1972) first described the impeller friction or disc friction losses.He is an experimental examiner. These losses, impeller input losses and impeller. He categorized it by dividing it into two as frictions in it. in the wheel frictions resulted in flow delay and pressure loss.Wing explaining the effect of the number of wings on the energy transfer, Bruno determined the optimum number of wings.

Balje (1981) produced a formula that gives proved that optimum efficiency in centrifugal fans can be achieved with slightly backward inclined impellers. In addition, it has revealed important findings in the literature on the slip factor.

Stodola (1945) revealed about methods for slip factor approximation. He proved that correlation between the slip factor and number of blades directly and he proved that average direction of discharge varies from the blade outlet angle due to number of blades, and also relative circulation in vane to vane plane. This situation can be cause the reduction in output values.

Kovatz and Desmur (1958) explained that the friction losses in the channels are a function of viscosity and this is directly proportional to the Reynolds number. He said that when the fluid reaches a turbulent structure, the wall roughness should also be included in the losses. In addition, due to the friction of the fluid disc rotating between the impeller and the volute and the turbulence. Friction losses are approximately 50% more than the normal duct friction losses. Other losses in the volute were also revealed by the surface roughness and the approach of the fluid to its walls, which in turn determined the yield of the volute.

Vibhakar (2012) conducted calculations using three different methods in his thesis study and compared them. One of these methods was based on fundamental principles, another was based on Church's approach, and the third was based on Osborne's method. Additionally, he performed a volute calculation by incorporating each study.

Shah and et all (2003) designed the unified design procedure after evaluating the performance of explicit designs, which were derived from the fundamental principles of fluid flow with minimal assumptions, as well as from Church, Osborne, and fundamental principles, which exhibited substantial differences. Additionally, they conducted a comparative evaluation of forward and backward-leaning radial-tipped

Stepanoff (1962), draw attention to the importance of hydraulic losses. These losses are caused by friction and eddies/vortices. Separation between the flow and wall/skin changes direction and magnitude of the velocity of the flow.

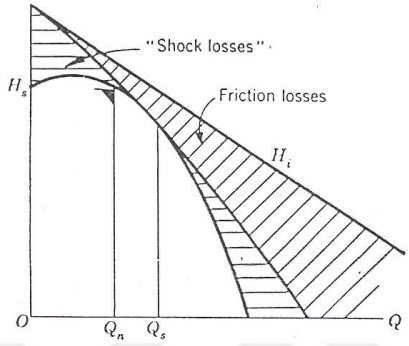


Figure 2.1. Q-H curves with losses

Osborne (1982) claimed that observation of actual performance of a centrifugal fan could be different from calculated by Euler equation. This difference can explain with circulation between the blades. Other factors that can cause the reduction in output values are volumetric leakage, pressure losses and mechanical losses also effect fan parameters.

Onma and Chantrasmi (2018) systematically investigated a numerical approach in their study to obtain performance curves of a backward-curved centrifugal fan using Computational Fluid Dynamics (CFD). They employed two different methods, with the first method incrementally changing the mass flow rate through the inlet boundary condition, and the second method utilizing a series of meshes representing the physical damper blade at various angles. They compared the results of both methods with an experimental setup in accordance with the AMCA fan performance testing standard.

Amjadimanesh and et all (2015) conducted a study to investigate the influence of blade count on the performance of a 3D forward-curved centrifugal fan. In their numerical analysis, they used the finite volume method to solve the governing equations and validated their numerical results with experimental data.

Yan and et all (2010) laid the foundation by investigating the selection methods and regularity of main parameters of numerous existing high-performance centrifugal fans. They proposed a new method for determining the main geometric parameters of the centrifugal fan's

impeller by establishing the relationships between specific speed and specific diameter, as well as between specific speed and the blade exit width.

Bamberger and Carolus (2017) proposed a new method for the design of centrifugal fan impellers with backward-curved blades. Unlike classical methods, they obtained seven correlations determining the geometric impeller parameters from aerodynamic optimization. Their objective was to maximize the total-to-static efficiency while precisely matching the targeted design points.

Lee and et all (2011) proposed a method for the redesign of a centrifugal impeller and its inlet duct in their study. Their aim was to reduce the power required to operate the fan without changing the volute exit pressure. To achieve this goal, they utilized experimental steering techniques with numerical optimization to redesign the fan blades, inlet duct, and impeller casing.

Kim and et all (2010) investigated the effect of the fan volute on performance based on changes in radial velocity.

Hildebrandt and Genrup (2007) conducted a numerical investigation using Computational Fluid Dynamics (CFD) to examine the effect of different exit angles in their study.

Ch and et all (2023) modeled a fan to reduce energy consumption and increase efficiency in response to the energy crisis. They examined the effect of different blade numbers on performance.

Ding and et all (2020) examined five different impeller models by comparing their volumetric flow rates at different blade outlet angles using Computational Fluid Dynamics (CFD).

Meng and et all (2012) investigated the effects of inlet angle, blade outlet angle, and blade number on the aerodynamic performance of a backward-curved centrifugal fan, considering the entire impeller-volute configuration.

Behzadmer and et all (2006) conducted a design of experiments to examine the efficiency of a backward-inclined centrifugal fan. In this study, they investigated parameters including the base radius of the motor hub, the radius of the fan entry section, the deceleration factor throughout the entry zone, and the solidity factor.

Karanth and et all (2010) aimed to explore the effect of boundary layer suction slots on various geometric positions on the impeller and on the diffuser using Computational Fluid Dynamics (CFD). They believed that the overall efficiency of the diffusion process in centrifugal fans could be enhanced by introducing boundary layer suction slots.

Rong and et all (2015) conducted a study where they found that the geometry of the channel through which the flow passes can lead to flow separation and subsequent energy loss. They applied the slotted technique by creating slots on the fan blades using CFD and concluded that the slotted model helps control and reduce boundary layer separation, thereby enhancing blade aerodynamic performance.

Myles (1969) conducted tests on five centrifugal fan impellers with five different blade structures, running at a constant speed in a specific volute, to analyze their losses. By correlating impeller and volute losses, expressed as a fraction of the dynamic exit pressure relative to the impeller

and volute, respectively, with a diffusion factor over a wide range of volume flow, the results were applied to other impellers and volutes.

3. MATERIAL AND METHOD

Austin church has been a pioneer in fan design studies by considering compressibility, temperature, pressure changes, losses. **(Church, 1947)**

In the experimental set used by Vibhakar in his thesis, he used the design methods of W. C. Osborne, Eck Bruno and D. J. Myles together with Church and showed them by comparing the experimental results in Figure 3.1. When the results shown in Figure 3.1 are analyzed, it is seen that Church's methodology gives the closest values to the experimental results in the assumptions of pressure and leakage losses, so the design with this methodology is preferred.

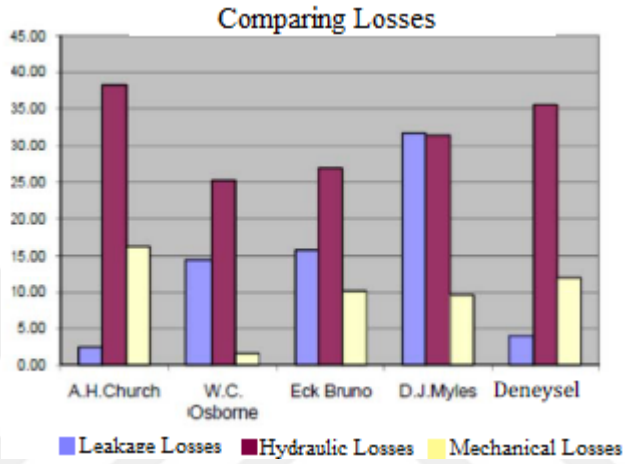


Figure 3.1. Comparison of losses in different design methods with experimental results (Vibhakar, 2012)

3.1. Velocity Diagrams

In order to understand the flow in the rotor, the difference between the velocities of moving objects It is necessary to understand the relationship well. Two concepts should be well known here, "relative" and "absolute" speed.

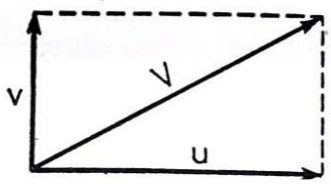


Figure 3.2. Relative and absolute velocities (Church, 1947)

For a rotating impeller, u is the velocity of the point on the impeller with respect to the ground, v is the relative velocity of the fluid with respect to the impeller and V is the absolute velocity of the fluid. Similarly, if we draw the velocity triangles for the impeller with a backward curved blade structure, we see the situation in Figure 3.3. Unlike here, only radial velocities are shown with V_r. The picture on the left in Figure 3.4 shows the cross-section of the impeller on the right. The fluid entering the impeller parallel to the axis of rotation rotates 90^0 after rotation enters the impeller blade

with a speed V_{r1} perpendicular to the axis. Then perpendicular to the axis of rotation (from the center outwards in the picture on the right), the continuing fluid is centrifugal with the effect of the force, it reaches V_{r2} speed at the blade exit.

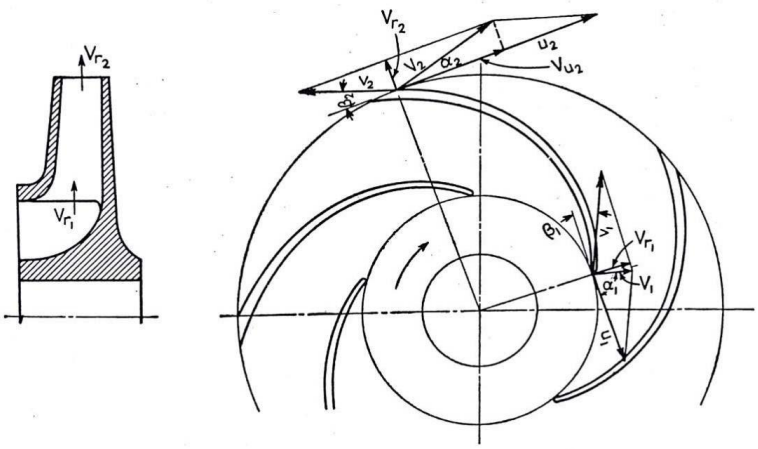


Figure 3.3. Inlet and outlet speed diagrams of single suction backward inclined vane impeller (Church, 1947)

The first region where the flow meets the blade is called point 1 and the region where it leaves the blade is called point 2. Firstly, the tangential velocity coming from the rotation speed is called "u_1" and the velocity tangent to the blade, which makes an angle "β_1" with the tangent due to the shape of the wheel and will direct the fluid, is called "v_1". The combination of these two vectorial velocities is "V_1". As seen in Figure 3.3, the angle made by the velocity "V_1" with the vector "u_1" is "α_1". If the same method is applied at point 2, the velocity triangle will be as shown in Figure 3-4. Finally, the velocity triangles are completed when the velocities "V_r", which will occur due to centrifugal force, are placed in the triangles perpendicular and outward to the axis of rotation. The locations of the velocity triangles formed during the movement of the fluid particle on the rotating impeller are shown in Figure 3.4 in the impeller cross-section

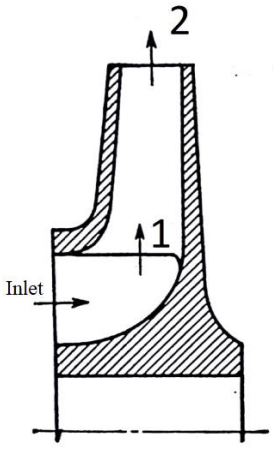


Figure 3.4. Impeller sections (Church, 1947)

Definition of the symbols on the velocity diagram

u_1 : Tangential velocity of the point at the blade inlet of the impeller relative to the ground

v_1 : Relative velocity of the fluid point at the blade inlet of the impeller relative to the impeller

β_1 : The angle between the direction u_1 and v_1

V_1 : Absolute velocity of the fluid point relative to the ground

α_1 : Angle between V_1 and u_1

V_{r1} : Radial component of velocity V_1

V_{u1} : Axial component of velocity V_1

u_2 : Tangential velocity of the point at the blade exit of the impeller relative to the ground

v_2 : Relative velocity of the fluid point at the blade outlet of the impeller with respect to the impeller

β_2 : The angle between the direction u_2 and v_2

V_2 : Absolute velocity of the fluid point relative to the ground

α_2 : Angle between V_2 and u_2

V_{r2} : Radial component of velocity V_2

V_{u2} : Axial component of velocity V_2

3.2. Losses

While applying the theoretical formulas, some assumptions are made such as frictionless, turbulence-free and the assumption that the fluid moves completely in accordance with the blades (infinite number of blades). But in reality, there are losses such as friction, turbulence, disc friction, leakage, mechanical losses due to these effects in the fan. In determining and formulating these losses and using coefficients many researchers have CFD an impact on the fixation. Stodola **(Stodola,1945)** was the first to formulate the effect of the rotation of the wheel on the flow between the blades.

The vectors shown with "Through Flow" in the region between the upper two wings in Figure 3.5 show the movement of the fluid between these wings without rotational effect. The vector shown with "Rotational Flow" is the vector describing the rotational effect in the region between the lower two wings. The combination flow is the combined vectors of straight flow and rotational flow.

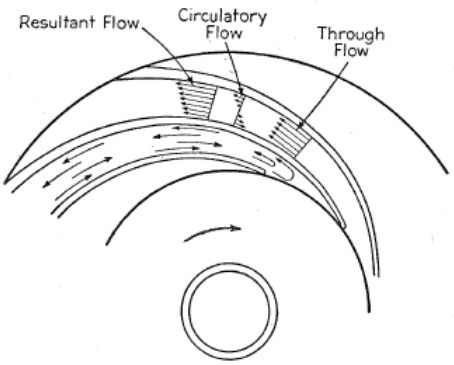


Figure 3.5. Rotational Flow, Straight Flow and its Combination (Church, 1947)

The velocity triangles occurring in the impeller inlet and outlet regions are changed with the rotation effect shown in Figure 3.5. The changed speed triangles are shown in Figure 3.6.

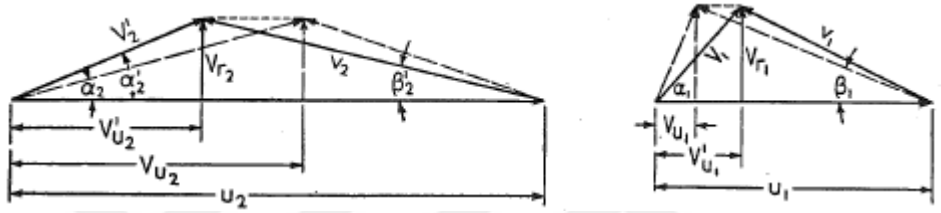


Figure 3.6. Inlet and Outlet Velocity Diagrams with Circulatory Flow Correction (Church, 1947)

According to Stodola, the tangent outlet velocity vector V_{u2} in the velocity triangle decreases by Wz due to the mentioned rotational effect. This amount is found by the following formula (Stodola, 1945).

$$Wz = \frac{\pi u2 \sin \beta 2}{z} \tag{3.1}$$

Wz : Losses from circulatory flow correction

Π : Pi number

u_2 : Tangential velocity at the outlet of impeller

β_2 : Blade outlet angle

z : Number of Blade

This formula was later confirmed by Kearton's **(Kearton, 1942**) experiments (rotation of the wheel the existence of a change in the velocity triangles with the effect of the velocity triangles) has been confirmed. This and similar other losses (friction, turbulence, disc friction, leakage losses, mechanical losses etc.) would be taken into account during the design methodology.

3.3. Design Methodology

The design methodology consists of 6 steps. These are; impeller design, volute design, losses (hydraulic loss, leakage loss and power losses), efficiencies, ideal shaft power required to rotate the fan and shaft diameter calculation **(Church, 1947)**.

3.3.1. Impeller Design

While the volumetric flow rate is constant, since the density will change depending on temperature and pressure, the mass flow rate will change accordingly. The density of air is calculated using the ideal gas equation in the 1st law of thermodynamics.

$$\rho_{atm} = \frac{P_{atm}}{RT_{atm}} \tag{3.2}$$

ρ_{atm} : Density of air at atmospheric Pressure [kg/m^3]
P_{atm} : Atmospheric Pressure [Pa]
R : Ideal gas constant [Nm/molxK]
T_{atm} : Temperature of Fluid in Kelvin at Atmospheric Pressure [K]

Blade inner section circle and inlet diameter

The circle with the distance from the center of the impeller to the point where the fluid first touches the impeller as it travels from the inside to the outside of the impeller is called the inner division circle, and the distance from the center to the point where the fluid leaves the impeller is called the outer division circle. A prediction is made for the channel cross-sectional velocity (V channel) perpendicular to the flow velocity on the suction side and the diameter of the suction channel cross-section is calculated as follows using the continuity equation of the fan at the desired flow rate.

$$Q = \frac{\pi D_{channel}^2}{4} V_{channel} \tag{3.3}$$

Q : Flow rate of air at the inlet [kg/m^3]
$D_{channel}$: Diameter of channel inlet [m]
$V_{channel}$: Velocity of channel inlet [m/s]

$$D_{channel} = \sqrt{\frac{4Q}{\pi V_{channel}}} \tag{3.4}$$

To find the Head at the impeller inlet, the air must be we use the kinetic energy in the total energy in the region. For this purpose, if we subtract the pressure and height differences from the Bernouilli equation, the velocity charge remains.

$$H=\frac{P}{\rho}+\frac{V^2}{2g}+z \rightarrow H=\frac{V^2}{2g} \quad (3.5)$$

H : Head [m]

In practice, the impeller inlet diameter (Fig. 3.4) usually corresponds to the channel inlet diameter. are equal and therefore the channel velocity (V channel) and the impeller inlet velocity (V inlet) are the same.

$V_{inlet}=V_{channel}$

In this case, the energy of the air at the impeller inlet in meters of water column unit is found by the formula below.

$$H=\frac{V_{inlet}^2}{2g} \quad (3.6)$$

The absolute static pressure at the impeller inlet is calculated by the following equation.

$$P_{inlet} = P_{atm} - P_{static} \quad (3.7)$$

P_{atm} : Atmospheric Pressure [Pa]
P_{inlet} : Inlet Pressure [Pa]
P_{static} : Static Pressure [Pa]

If defined by pressure ratios ε_p, the ratio of the impeller inlet pressure to the atmospheric pressure is given in the equation below.

$$\varepsilon_p = \frac{P_{inlet}}{P_{atm}} \quad (3.8)$$

ε_p : Pressure ratio

The ideal gas equation;

$$PV=mRT \tag{3.9}$$

P	: Absolute Pressure	[Pa]
V	: Volume	[m^3]
m	: Weight of air	[g]
R	: Air constant	[J/Kmol]
T	: Absolute temperature	[K]

Since the work to be done in the fan (w) will be with the pressure increased by compressing at constant volume, it is shown by the following equation.

$$w = -\int_a^b vdP \tag{3.10}$$

The following formula is used for isentropic (constant entropy, no heat transfer) state change.

$$Pv^k = C = constant \tag{3.11}$$

$$k = \frac{c_p}{c_v} \tag{3.12}$$

c_p	: Specific heat at constant pressure	[J/gK]
c_v	: Specific heat at constant volume	[J/gK]
P	: Static Pressure	[Pa]
v	: Air velocity	[m/s]
c	: constant	[-]

The American Society of Mechanical Engineering standard for centrifugal compressors is 36% humidity and 68 ^{0}F for air (Church,1947).

$$k=1.3947 \tag{3.13}$$

If we equalize the two states, a being the initial state and b being the second state, the following equation is obtained by adapting formula (3.11).

$$P_b V_b^k = P_a V_a^k \tag{3.14}$$

From Equation (3.9) and (3.14) the following equation is obtained.

$$P_b = P_a \left(\frac{V_a}{V_b}\right)^k = \frac{WRT_b}{V_b} \tag{3.15}$$

$$V_b = V_a \left(\frac{P_a}{P_b}\right)^{\frac{1}{k}} = \frac{WRT_b}{P_b} \tag{3.16}$$

From equation (3.9);

$$\frac{P_a V_a}{P_b V_b} = \frac{T_a}{T_b} \Longrightarrow T_b = \frac{T_a P_b V_b}{P_a V_a}$$

Now if V_b is replaced by equation (3.16);

$$T_b = \frac{T_a P_b V_a \left(\frac{P_a}{P_b}\right)^{\frac{1}{k}}}{P_a V_a} = T_a\left(\frac{P_b}{P_a}\right)\left(\frac{P_a}{P_b}\right)^{\frac{1}{k}} = T_a\left(\frac{P_b}{P_a}\right)\left(\frac{P_b}{P_a}\right)^{-\frac{1}{k}} = T_a\left(\frac{P_b}{P_a}\right)^{1-\frac{1}{k}}$$

$$T_b = T_a\left(\frac{P_b}{P_a}\right)^{\frac{k-1}{k}} \tag{3.17}$$

With equation (3.13);

$$\frac{k-1}{k} = 0.283 \tag{3.18}$$

Thus, equation (3.17) becomes as follows;

$$T_b = T_a\left(\frac{P_b}{P_a}\right)^{0.283}$$

Now, if we accept “a” as the state at atmospheric pressure and “b” as the state at the impeller inlet (Figure 3.4.); the following equation is written and when equation (3.8) is substituted, the following equation is obtained from equation (3.19).

$$T_{inlet} = T_{atm}\left(\frac{P_{inlet}}{P_{atm}}\right)^{0.283} \tag{3.19}$$

$$T_{inlet} = T_{atm}(\varepsilon_{pinlet})^{0.283} \ (^0K) \tag{3.20}$$

The density of the air at the impeller inlet indicated in (Figure 3.4) is calculated by the following formula.

$$\rho_{inlet} = \frac{P_{inlet}}{RT_{inlet}} \ (Kg/m^3) \tag{3.21}$$

Using the above equations, the volumetric flow rate at the impeller inlet is found.

$$\dot{m} = Q_{inlet} \, x \, \rho_{inlet} \quad (kg/s)$$

$\dot{m}$: Mass flow rate [kg/s]

$$Q_{inlet} = \frac{\dot{m}}{\rho_{inlet}} \qquad [m^3/s] \tag{3.22}$$

Equation (3.23) is obtained using the following equation for the impeller inlet diameter.

$$Q_{inlet} = V_{inlet} \frac{\pi D^2}{4}$$

$$D_{inlet} = \sqrt{\frac{4}{\pi}} x \sqrt{\frac{Q}{V_{inlet}}} \tag{3.23}$$

Blade Inlet Parameters

The blade inlet diameter should be slightly larger (Church, 1947).

$$D_1 = 1.02 D_{inlet} \tag{3.24}$$

The circumferential tangential velocity at the blade inlet is expressed by the following equation.

$$u_1 = \frac{\pi D_1 N}{60} \tag{3.25}$$

u_1 : The circumferential tangential velocity at the blade inlet [m/s]

D_1 : Blade inlet diameter [m]

N : Rotation of impeller [rpm]

Blade radial inlet velocity V_1, 5 % more than V_{inlet} (Church,1947)

$$V_1 = V_{r1} = 1.05 V_{inlet} \tag{3.26}$$

When the fluid, which is assumed to enter the impeller inlet perpendicularly, is assumed to enter the blade at 90^0, that is, when the angle α1 is accepted as 90^0, the following equation is written from the velocity triangle at the blade inlet and the angle β1 is calculated from the right triangle.

$$\tan \beta_1 = \frac{V_{r1}}{u_1} \tag{3.27}$$

β_1 is increased by 3% to take into account flow breaks at the inlet (Church, 1947).
Assuming $\alpha_1 = 90'$, the blade inlet relative speed is calculated according to the triangle in Figure 3.3 by the following formula.

$$v_1^2 = u_1^2 + V_1^2$$
$$v_1^2 = (u_1^2 + V_1^2)^{\frac{1}{2}} \tag{3.28}$$

When calculating the blade inlet area (A_1), the volumetric flow rate (Q_{inlet}) is increased by 3% due to leakage losses **(Church, 1947)**. Thus, the impeller blade area is calculated by the following equation.

$$A_1 = \frac{1.03\, Q_{inlet}}{V_1} \tag{3.29}$$

In order to define a thickness correction factor ($\acute{\varepsilon}_1$) considering the wing thicknesses in the wing inlet area, the following equation is obtained by subtracting the areas of the wing thicknesses from the blade inlet area.

$$A_1 \dot{\varepsilon}_1 = A_1 - \frac{t}{\sin \beta_1} b_1 Z \tag{3.30}$$

$\acute{\varepsilon}_1$: Blade inlet area thickness correction factor
b_1 : Blade inlet width [m]
t : Blade thickness [mm]
β_1 : Blade inlet angle [^{0}]
Z : Blade number

$$\dot{\varepsilon}_1 = \frac{A_1}{A_1} - \frac{t b_1 Z}{\sin \beta_1 A_1} = 1 - \frac{t b_1 Z}{\sin \beta_1 (\pi D_1 b_1} = 1 - \frac{tZ}{\sin \beta_1 \pi D_1} \tag{3.31}$$

$$A_1 = b_1 \pi D_1 \dot{\epsilon}_1$$

$$b_1 = \frac{A_1}{\pi D_1 \dot{\epsilon}_1} \tag{3.32}$$

Impeller Outlet Parameters

If Equations (3.9), (3.10) and (3.11) are taken into account and a and b in Equation (3.10) are considered as "input" and "2" states respectively and their integral is solved **(Çengel and Boles, 1996),** the following equation is obtained.

$$w = \frac{kR(T_{inlet} - T_2)}{k-1} = \frac{kRT_{inlet}}{k-1}\left[\left(\frac{P_2}{P_{inlet}}\right)^{k-1/k} - 1\right] \tag{3.33}$$

If we divide this work by the inlet volume, we find the adiabatic compression height created along the impeller.

$$\frac{w}{v_{inlet}} = H_{ad} \tag{3.34}$$

If we drop "v" from Equation (3.9) and substitute it in Equations (3.33) and (3.34), the following equation is obtained.

$$H_{ad} = \frac{\frac{kRT_{inlet}}{k-1}\left[\left(\frac{P_2}{P_{inlet}}\right)^{k-1/k} - 1\right]}{\frac{RT_{inlet}}{P_{inlet}}} = \frac{P_{inlet}}{\frac{k-1}{k}}\left[\left(\frac{P_2}{P_{inlet}}\right)^{k-1/k} - 1\right] \tag{3.35}$$

Pressure ratios are defined as in equation (3.36).

$$\epsilon_{p_{impeller}} = \frac{P_2}{P_{inlet}} \tag{3.36}$$

With equation 3.18 3.34 and 3.35 the following equation is obtained.

$$H_{ad} = \frac{RT_{inlet}}{0.283g}\left[\epsilon_{P_{impeller}}^{0.283} - 1\right] \tag{3.37}$$

Church (1947) formulated the total pressure height created in the impeller by energy transfer as follows.

$$H_{ad} = \frac{K' u_2^2}{g} \tag{3.38}$$

There;

$$u_2 = \frac{\pi D_2 N}{60} \tag{3.39}$$

H_{ad} : Adiabatic Head [m]

u_2 : Velocity of Blade outlet [m/s]

D_2 : Impeller outside diameter [m]

N : Revolution of Impeller

K^1 : Constant. Church found this value between 0.5 and 0.65 by experiments. While we calculate the outlet diameter of the impeller, K' value will be used by accepting 0,58 initially.

$$H_{ad} = \frac{K'}{g}\left(\frac{\pi D_2 N}{60}\right)^2$$

$$D_2 = \frac{60}{\pi N}^2 \sqrt{\frac{g H_{ad}}{K^1}} \tag{3.40}$$

$$u_2 = \frac{\pi D_2 N}{60} \tag{3.41}$$

The radial outlet velocity (V_{r2}) is lower than the input velocity due to sudden speed variations along the impeller. (V_{r1}) 15% will be taken small **(Church, 1947)**.

$$V_{r_2} = 0.85 V_{r_1}$$

$$V_{u_2} = u_2 - \frac{V_{r_2}}{\tan \beta_2} \tag{3.42}$$

If we subtract Stodola' s loss formula from V_{u2}, taking into account the loss of the rotation effect, the loss tangential exit velocity is found as follows.

$$V'_{u_2} = V_{u_2} - W_z$$

$$V'_{u_2} = V_{u_2} - \frac{\pi u_2 \sin \beta_2}{z} \tag{3.43}$$

Recalling that the straight lines in the velocity triangle in Figure 3.6 are vectors that change with rotation (loss velocities, represented by letters with exponents), the absolute velocities (V_2', v_2) and angles (α_2') at the exit are respectively formulated as follows.

$$V_2'^2 = V_{r_2}^2 + V_{u_2}'^2$$
$$V_2' = \sqrt[2]{V_{r_2}^2 + V_{u_2}'^2} \quad (3.44)$$

$$v_2^2 = V_{r_2}^2 + \left(u_2 - V_{u_2}\right)^2$$
$$v_2 = \sqrt[2]{V_{r_2}^2 + \left(u_2 - V_{u_2}\right)^2} \quad (3.45)$$

$$\tan \alpha_2' = \frac{V_{r_2}}{V_{u_2}'} \quad (3.46)$$

The theoretical head created by the impeller and free from friction, rotational effect and turbulence is calculated by the following equation.

$$H_{theorical} = \frac{1}{2g}(u_2^2 - u_1^2 + v_1^2 - v_2^2) \quad (3.47)$$

The compression head due to the centrifugal effect is expressed as follows.

$$\frac{u_2^2 - u_1^2}{2}$$

The compression head due to the relative velocity effect is expressed as follows.

$$\frac{v_1^2 - v_2^2}{2}$$

15% of the theoretical pressure the rotational effect in the impeller is lost due to the effect of friction and turbulence **(Church, 1947).**

$$H_{effective} = 0.85\, H_{theorical} \quad (3.48)$$

Since the impeller outlet pressure depends on this effective head, equation (3.37) is rearranged for the blade inlet and outlet (Fig. 3.4. "Inlet" and "2").

$$\left(\epsilon_{P_{impeller}}^{0.283} - 1\right) = \frac{0.283g(H_{effective})}{RT_{inlet}} \quad (3.49)$$

$\epsilon_{P_{impeller}}$: Effective pressure ratio between impeller inlet and impeller outlet.

$$\epsilon_{P_{impeller}} = \frac{P_2}{P_{inlet}} \Longrightarrow P_2 = \epsilon_{P_{impeller}} x P_{inlet} \quad (3.50)$$

Since friction and turbulence losses are converted into heat, this increases the temperature of the fluid slightly. If we neglect the losses, the impeller outlet temperature increases at the rate of adiabatic pressure in the impeller. We apply the adiabatic head to Equation (3.47) and calculate $\epsilon_{P_{impeller}}^{0.283}$ value.

$$\left(\epsilon_{P_{impeller}}^{0.283} - 1\right) = \frac{0.283gH_{ad}}{RT_{inlet}} \quad (3.51)$$

To find the outlet temperature, T_2 is calculated from formula (3.20).

$$T_2 = \epsilon_{P_{impeller}}^{0.283} x T_{inlet} \quad (3.52)$$

The density of the fluid at the impeller outlet is obtained from the following equation.

$$\rho_2 = \frac{P_2}{RT_2} \quad (3.53)$$

If we increase the flow at the outlet of the impeller by 3% **(Church, 1947),** taking into account 3% leakage losses, the volumetric flow rate at the outlet is obtained by the following equation.

$$Q_{outlet} = 1.03 x Q_{inlet}/\rho_2 \quad (3.54)$$

The impeller outlet area is calculated by the equation expressed below.

$$A_2 = \frac{Q_{outlet}}{V_{r_2}} \quad (3.55)$$

The outlet blade thickness factor is calculated using equation (3.30) as follows.

$$\varepsilon_2 = 1 - \frac{tZ}{\sin\beta_2 \pi D_2} \quad (3.56)$$

The blade exit height b_2 is calculated by the following equation.

$$b_2 = \frac{A_2}{\pi D_2 \varepsilon_2} \tag{3.57}$$

3.3.2. Volute Design

Rather than the Trapezoidal volute structure proposed by Church, a rectangular section volute was proposed for ease of production and ease of calculation. (Figure 3.7)

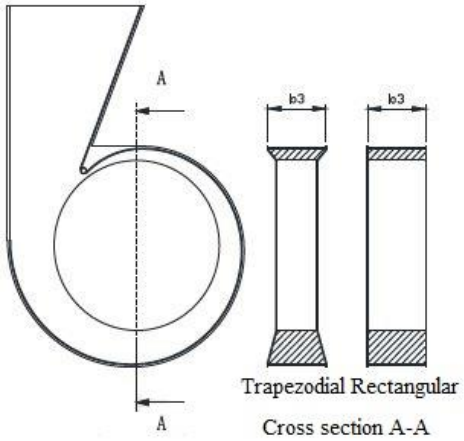


Figure 3.7. Volute Cross Section

The various air streams leaving the blade tips are collected in the scroll housing and reunited into a single air stream that leaves the unit at right angle to the axis. This method of scroll casing design is known as 4-point method. The radii at different cross section are correlated with impeller exit diameter.

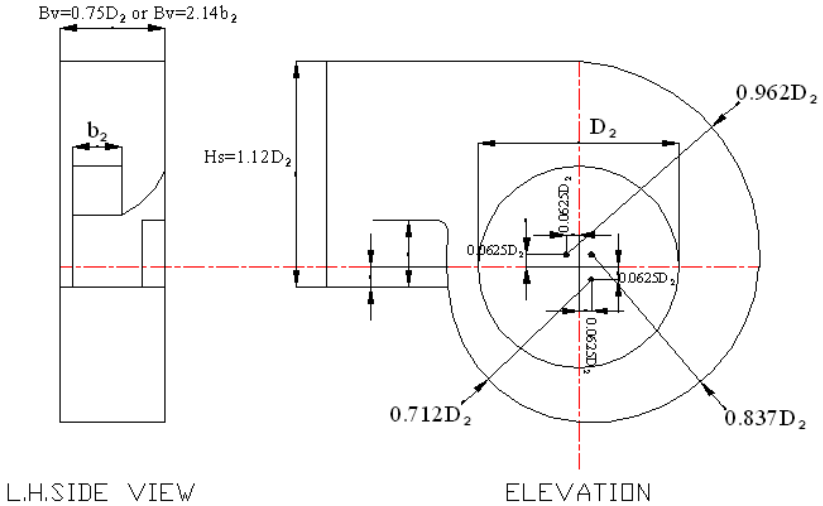


Figure 3.8. Scroll Casing Design by 4 Point Method (Vibhakar,2015)

$$b_3 = 2.14 x b_2 \quad (3.58)$$

b_3: Volute back width [mm]

$$SC_{r31} = 71.2\ \%\ \text{of}\ D_2 \quad (3.59)$$

$$SC_{r32} = 83.7\ \%\ \text{of}\ D_2 \quad (3.60)$$

$$SC_{r33} = 96.2\ \%\ \text{of}\ D_2 \quad (3.61)$$

Centre of thee three are located off the center lines by interval of %6.25 of D_2.

$$\text{Center of dia} = 6.25 * D_2 \quad (3.62)$$

$$H_v = D_2 * 1.12 \quad (3.63)$$

$$R_t = 1.075\ R_2 \quad (3.64)$$

$$Q_t = 132 \log(\frac{R_t}{R_2}) / \tan \alpha'_2 \quad (3.65)$$

$A_v = (1\text{-}0.35) * H_v * b_v$ (3.66)

$V_4 = Q_{out} / A_v$ (3.67)

H_v	: Height of Volute	(m)
R_t	: Radius of Tongue	(m)
Q_t	: Volute tongue angle	(^{0})
A_v	: Exit volute area	(m^2)
V_4	: Outlet velocity of casing	(m/s)

3.3.3. Losses

Leakage Losses

Some leakage in the gaps between the impeller and the volute loss and a loss of 3% is calculated as follows (Church, 1947).

$$Q_L = 0.003 \text{ x } Q \tag{3.68}$$

Suction Pressure Losses

The losses due to friction and turbulence at the impeller inlet are expressed by the following equation. Here, the loss coefficient k_i is selected between 0.5 and 0.8 **(Osborne, 1977).** In this study, 0.65 will be taken.

$$dP_{suction} = \frac{1}{2} x k_i x \rho_{inlet} x V_{inlet}^2 \tag{3.69}$$

Impeller Pressure Losses

Here, since the blades used in the design are made of sheet metal, the k_{ii} is selected between 0.2-0.3 **(Osborne, 1977).** It will be evaluated as 0.25.

$$dP_{impeller} = \frac{1}{2} k_{ii} \rho_{inlet} (v_1 - v_2)^2 \tag{3.70}$$

Disc Friction Loss

$$T_{df} = \pi f \rho w_2^2 \frac{R_2^5}{5} = \pi f \rho_2 (\frac{U_2}{R_2})^2 \frac{R_2^5}{5} \tag{3.71}$$

f	: friction constant	
ρ	: density of fluid	[kg/m^3]
ω	: angular velocity of impeller	[rad/s]
R_2	: Outlet radius of impeller	[m]
U_2	: Impeller outlet tangential velocity	[m/s]

The material friction coefficient f is taken as 0.005 for steel sheets. Thus, the power loss due to disc friction is found by the following equation (Osborne, 1977).

$$P_{df} = \frac{2\pi N(T_{df})}{60} \tag{3.72}$$

Volute Pressure Loss

$$dP_{vc} = k_{iii} x \frac{1}{2} x \rho_2 x (V_2' - V_4)^2 \quad (3.73)$$

k_{iii} : 0.4

3.3.4. Efficiencies

Hydraulic Efficiency

$$\eta_{hyd} = \frac{\Delta P}{\Delta P + dP_{suc.} + dP_{imp.} + dP_{.Volute}} \quad \textbf{(Church,1947)} \quad (3.74)$$

Volumetric Efficiency

$$\eta_{volumetric} = \frac{Q}{Q+Q_L} \quad \textbf{(Church,1947)} \quad (3.75)$$

Total Efficiency

$$\eta_{total} = \eta_{hyd.} + \eta_{volumetric} \quad \textbf{(Church,1947)} \quad (3.76)$$

3.3.5 Ideal Shaft power required to run the fan

$$W = \frac{(\Delta P + dP_{suc.} + dP_{imp.} + dP_{volute})(Q+Q_L)}{\eta_{total}} + P_{df} \quad \textbf{(Church,1947)} \quad (3.77)$$

$$\tau_{df} = \frac{Wx60}{2\pi x 2800} \quad \textbf{(Church,1947)} \quad (3.78)$$

3.4. Fan Design

The inputs of the fan of the snow ploughing and blowing vehicle of Koluman Automotive Industry (KOE) and the values of the fan to be designed at the same time are given below.

Volume flow rate at outlet (Q)	: 8.255 m^3/s
Diameter of Impeller (D_{uct})	: 800 mm
Density of air (ρ_{air})	: 1.02 kg/m^3
Atmospheric Pressure (Pa)	: 101325 Pa
Static Pressure at suction (Pa)	: 2300 Pa
Ideal Gas Constant (R)	: 287 (N.m)/(mol K)

Temperature of air at atm. Pressure (C^0) : 25^0

Gravity force (g) : 9.81 m/s^2

Rotation of Impeller (N) : 3200 rpm

Blade thickness (t) : 4 mm

Blade number (Z) : 13

Blade outlet angle (β_2) : 45.3 ^{0}

3.4.1. Calculations

The figures extracted using the formulae in Chapter 3 and the inputs and values of the fan will be inserted into an "Excel" worksheet. Then the new iteration values by adding the total value of the losses to the design pressure will be found. In the same way, the other variables will be and the iteration will continue until the difference is below 1%. The resulting values will be our desired design values.

The reason for choosing this fan in the study is that its characteristic curve is available, it is actively working at the airport and its improvement potential is seen. The CFD result of this fan will be compared with the CFD result of the fan designed with Church's calculation method and the ideal calculation method will be reached by updating the design. In order to make a healthy comparison, some assumptions have been made that the design method here also allows us. These are:

Blade outlet angle (β_2) : 45.3^O

Velocity inlet (V_{inlet}) : 63.3 m/s (Q_{inlet} is known and diameter of impeller inlet case (408mm)

$$V_{inlet} = \frac{4Q}{\pi D^2_{channel}} = 63.142 \text{ m/s}$$

$$\dot{m} = Q x \rho_{air}$$

The design methodology in Chapter 3 and the design inputs described in this chapter have been calculated using formulae and assumed figures and entered in Appendix A, Table 3.1 in the appendices at the end of this thesis.

Impeller Design

$H_{suction}$ is found by using equation (3.6) at impeller inlet with V_{inlet}: 63.142 m/s. The value of H would be 202.950 m.

Absolute static Pressure is obtained from equation (3.7) as 99025 Pa.

The ratio of the impeller inlet pressure to atmospheric pressure is found by using equation (3.8). The temperature at impeller inlet is obtained by using equation (3.20). By using this value, the air density

of impeller inlet is founded with equation (3.22). These results would be shared at the attachment as an Appendix A, Table 3.1.

Blade Inlet Parameters

First of all, D_1 would be obtain by using equation (3.24). After that, u_1 would be found from (3.25). Step by step the equations (3.26), (3.27), (3,28), (3,29) and (3,32) would be calculated. These result would be shared at the Appendix A, Table 3.1 end of this thesis.

Impeller Outlet Parameters

With equation (3.36) pressure ratio is calculated, if some assuming accepted like P_{outlet} is equal to P_{atm}. By using (3.37), $H_{adiabatic}$ is obtained. After this calculation D_2 is founded. The value of D_2 is used for calculating u_2 from (3.41). Then, V_{r2} is found by multiply the V_{r1} with 0,85. So that, V_{u2} is got from (3.42). Stodola's formula (3.1) is helped to find W_z. Now subtract the slip due to the rotation effect (W_z) from the tangent projection (V_{u2}) of the absolute exit velocity (V_2), the projection of the real absolute velocity (V'_{u2}) from equation (3.43). Absolute exit velocity V'_2 is from equation (3.44). Now the values of v_2, α'_2, H theoretical, and H effective are obtained by equations (3.45), (3.46), (3.47), and (3.48) respectively. Then, from equation (3.50) with $\varepsilon_{Pimp.}$ calculated with equation (3.49), P_2 is found. If the conversion of friction and turbulence into heat from the inlet to the outlet of the impeller is also taken into account, $\varepsilon_{P_{imp.}}^{0.283}$ is obtained from equation (3.51) and this figure is then substituted in equation (3.52) and T_2 is calculated. From here, the impeller outlet density, ρ_2, is found from equation (3.53). Depending on this density, the outlet flow rate Q_{output} is obtained from equation (3.54). Then A_2, $\acute{\varepsilon}_2$, and b_2 are calculated by using equation (3.55), (3.56), and (3.57) respectively, the blade thickness of 4 mm, and written in Appendix A, Table 3.1, 1st iteration column.

Volute Design Calculations

First of all, by using equation (3.58) b_3 is founded. Then diameters of Scroll casing are calculated from (3.59), (3,60), (3,61) respectively. After that center of these diameter is calculated by (3.62). Height of volute is obtained from equation (3.63). R_t is calculated from equation (3.64). With these data we create the first line of Annex A, Table 3.1. Finally, the volute throat angle Q_t are determined by the formula (3.65) and substituted in iteration 1 of the corresponding schedule. After all A_v and V_4 are calculated by equation (3.66) and (3.67) respectively.

Losses

In section 3.3.3.1, leakage loss is calculated by using the losses with equation (3.68).

In section 3.3.3.2, the suction pressure loss is calculated with equation (3.69). Impeller pressure loss is calculated from (3.70). Disc friction loss is obtained from equation (3.71). Then power loss due to disc friction and volute pressure loss are calculated by equation (3.72) and (3.73) respectively. After that hydraulic efficiency, volumetric efficiency and total efficiency are obtained from equation (3.74), (3.75), (3.76) respectively. Ideal shaft power required to run fan would be calculated from equation (3.77). From equation (3.78) required torque is obtained for running the fan. End of the calculations the results is written to Appendix A, Table 3.1.

Second Iteration Calculations

The 2_{nd} iteration is continued by adding the volumetric flow loss to the design values and the results obtained are written in the iteration 2 column in Appendix A, Table 3.1. By adding leakage losses to the flow rate in the 1st iteration, the new flow rate is calculated by equation 3.79 below.

$$Q_{2nd} = Q + Q_L \tag{3.79}$$

In section 3, the suction pressure, impeller pressure and volute pressure losses defined by equations (3.72), (3.73), (3.76) are added together to obtain the total pressure loss.

$$P_{losses} = dP_{suction} + dP_{impeller} + dP_{volute} \tag{3.80}$$

These losses are added to the pressure difference in the first stage to obtain ΔP_{2nd}.

$$\Delta P_{2nd} = \Delta P + P_{losses} \tag{3.81}$$

Since there will be an increase in flow rate due to the loss of volumetric flow rate, the mass flow rate is multiplied by the density of the air and recalculated with the equation below.

$$\dot{m}_{2nd} = Q_{2nd} \text{ x } \rho \tag{3.82}$$

$$Q_{2nd} = V_{duct} \left(\pi D^2_{duct\ 2nd}/4\right) \tag{3.83}$$

$$D^2_{duct\ 2nd} = Q_{2nd} * 4 \,/(\pi V_{duct}) \tag{3.84}$$

$$Q_{inlet\ 2nd} = \dot{m}_{2nd} \,/\, \rho_{inlet} \tag{3.85}$$

The calculations in section 3 are repeated using the new values determined as a result of the losses. The results obtained are written in the 2nd iteration column in Appendix A, Table 3.1. After the calculations were performed, the percentage difference between the iterations was checked. Since there was more than 1% difference, the 3rd iteration step was started. The results of the 3rd iteration were added to Appendix A, Table 3.1 in the relevant column. At the end of the 3rd iteration, since the difference between the results was observed to be less than 1%, the iteration step was terminated here. After iterations are completed, according to results summary information is given in Table 3.1.

Table 3.1.Designed Church fan impeller drawing schedule

	SYMBOL	**UNIT**	
Blade Outlet Angle	β_2	^{0}	45.3
Blade Inlet Angle	β_1	^{0}	46.38
Inlet Diameter	D_{inlet}	mm	387
Blade Inlet Diameter	D_1	mm	395
Blade Outlet Diameter	D_2	mm	593
Blade Inlet Width	b_1	mm	98.882
Blade Outlet Width	b_2	mm	74.017

The drawing of the impeller which is designed according to Church, is shown in Figure 3.9.

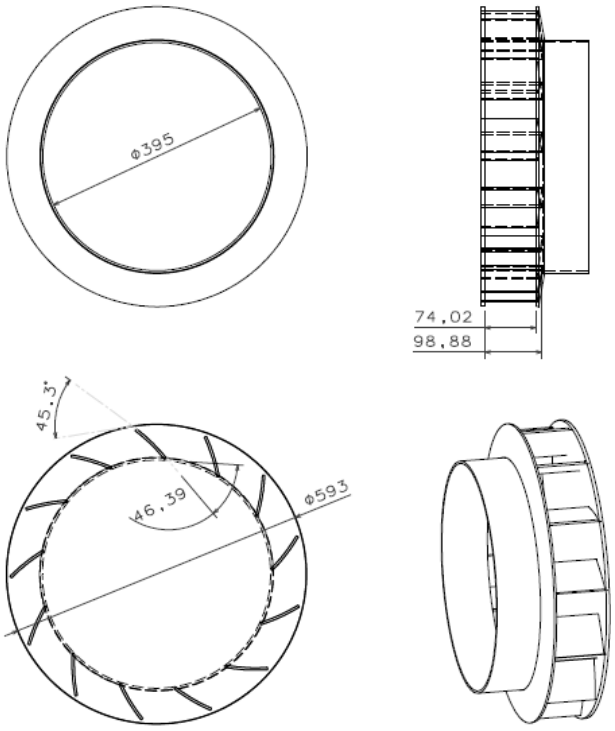


Figure 3.9. Drawing of impeller according to Church design

3.5. Comparison of the Fan

3.5.1. Comparison of Impeller

The technical drawing of the existing tested impeller is given in Figure 3.10.

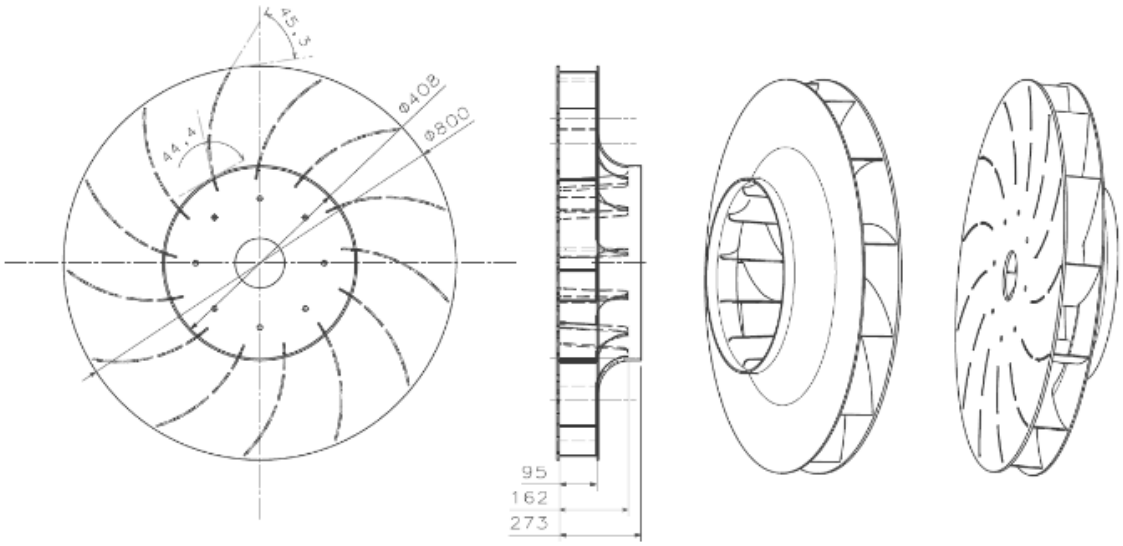


Figure 3.10. Drawing of the tested fan impeller

The comparison of the impellers between tested fan and designed fan values is shown in Table 3.2.

Table 3.2. Comparison of impellers

	SYMBOL	UNIT	CHURCH	KOE
Blade Outlet Angle	β_2	^{0}	45.3	45,3
Blade Inlet Angle	β_1	^{0}	46.38	44,4
Inlet Diameter	D_{inlet}	mm	387	414
Blade Inlet Diameter	D_1	mm	395	408
Blade Outlet Diameter	D_2	mm	593	800
Blade Inlet Width	b_1	mm	98.882	162
Blade Outlet Width	b_2	mm	74.017	95

After the exit angles of the blades were entered equally at the beginning of the design, there was a difference of about 4% between the inlet angles of the blades. Probably the difference arose due to the fact that the outer diameters were quite different. While the outer diameter of the impeller was calculated as 593 mm in the Church method, 800 mm was used in the outsourced design available at KOE.

Since the blade exit angle is a design value, it is written the same in both designs. The inlet diameters were different because they were designed with different methods. In the Church method,

a pipe of the same diameter is designed to directly enter the impeller, while in the snow plow fan, the diameter is narrowed by choosing a tapered channel from a larger diameter to the impeller inlet, and this design is a less loss design as it directs the flow. There was a difference of 13 mm in the blade inlet diameters.

In summary, when the impellers are compared, there is a 35% difference between the outer diameters of the impellers, a 64% difference between the blade inlet widths at b_1 and a 28% difference between the b_2 values. When the following fan law of **(Bleier, 1998)** is checked according to equations 3.86, 3.87, 3.88, illogical results appear. The relationship between impeller outer diameter change and volumetric flow rate, the relationship between impeller outer diameter change and static Pressure, the relationship between impeller outer diameter change and power are given below.

$$\frac{Q_2}{Q_1} = \left(\frac{D_2}{D_1}\right)^3 \tag{3.86}$$

$$\frac{P_2}{P_1} = \left(\frac{D_2}{D_1}\right)^2 \tag{3.87}$$

$$\frac{W_2}{W_1} = \left(\frac{D_2}{D_1}\right)^5 \tag{3.88}$$

Fan laws and how the difference between the Church fan impeller outer diameter and the KOE fan impeller outer diameter affects flow rate, pressure and power, respectively should have an impact.

$$\frac{Q_{Church}}{Q_{KOE}} = \left(\frac{D_{Church}}{D_{KOE}}\right)^3 \Rightarrow Q_{Church} = Q_{KOE}x\left(\frac{D_{Church}}{D_{KOE}}\right)^3 = 8.255x\left(\frac{0.593}{0.8}\right)^3 = 3.36\ m^3/s$$

According to the calculation, the output value was 7.46 m^3/s, while this value was obtained as 3.36 m^3/s in the control based on the fan laws.

$$\frac{P_{Church}}{P_{KOE}} = \left(\frac{D_{Church}}{D_{KOE}}\right)^2 \Rightarrow P_{Church} = P_{KOE}x\left(\frac{D_{Church}}{D_{KOE}}\right)^2 = 2300x\left(\frac{0.593}{0.8}\right)^2 = 1263.3\ Pa$$

$$\frac{W_{Church}}{W_{KOE}} = \left(\frac{D_{Church}}{D_{KOE}}\right)^2 \Rightarrow W_{Church} = W_{KOE}x\left(\frac{D_{Church}}{D_{KOE}}\right)^2 = 105x\left(\frac{0.593}{0.8}\right)^5 = 23.47\ kW$$

According to the Church calculation, 69.92 kW power consumption is available, while 23.47 kW power consumption is obtained according to Equation 3.88.

When these results were checked, it was decided that there was an error in the application or calculation and then the system was checked. It was ignored that only the fan and volute data were

available within the scope of the calculation, but in the tested product there is a twisted blowing duct at the outlet of the volute, and the duct has highly variable diameters and lengths. It is obvious that these physical differences will lead to losses and produce values that are quite different from the calculation. For this reason, the values were collected through the pitot tube without the blowing channel determined in the image below and a new flow rate and static pressure measurement were taken.



Figure 3.11. Tested fan with blowing unit

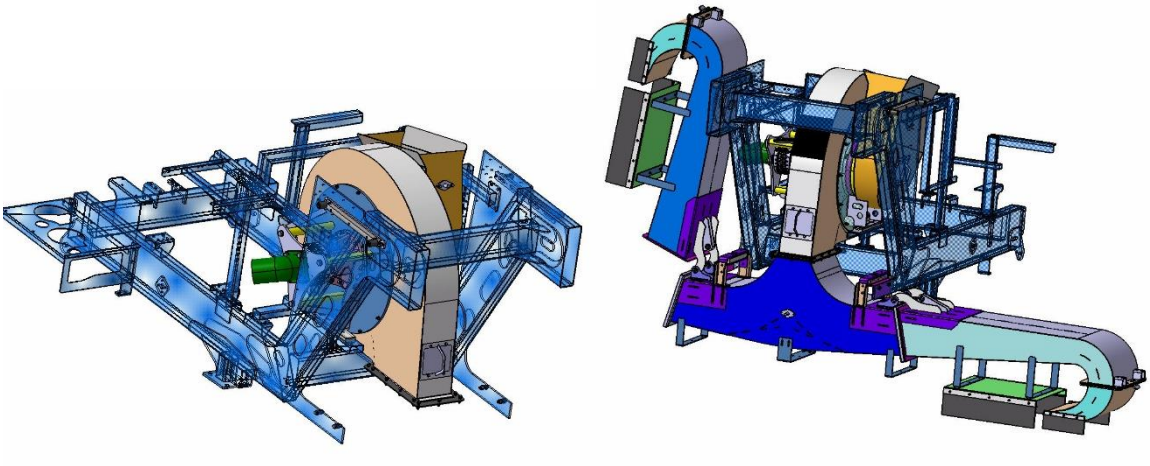


Figure 3.12. Tested fan without blowing unit

The inputs of the fan of KOE's snow plow and blower without the blowing channel and the values of the fan to be redesigned are given below.

Volume flow rate at outlet (Q) : 9.4 m^3/s

Static Pressure at suction (Pa) : 4200 Pa

When the calculations are repeated with the current inputs, the new values are presented in table 3.3.

Calculation results is shown in Appendix A, Table 3.2.

Table 3.3. Redesigned Church fan impeller drawing schedule

	SYMBOL	UNIT	
Blade Outlet Angle	β_2	^{0}	45.3
Blade Inlet Angle	β_1	^{0}	50.054
Inlet Diameter	D_{inlet}	mm	390
Blade Inlet Diameter	D_1	mm	398
Blade Outlet Diameter	D_2	mm	770
Blade Inlet Width	b_1	mm	99.193
Blade Outlet Width	b_2	mm	56.619

According to the data obtained as a result of the calculation, the wheel of the Church design was re-modelled using CATIA V5. The model technical drawing is shown in Figure 3.13.

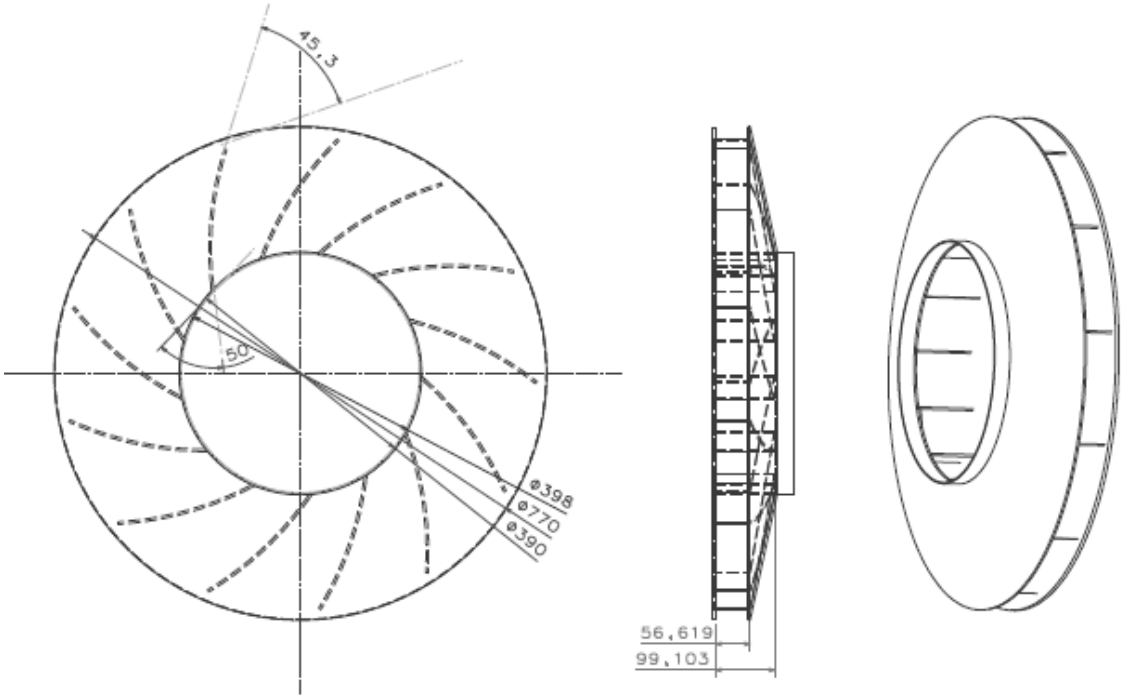


Figure 3.13. Church redesigned impeller

Table 3.4 is shown the comparison of the impellers between tested fan and redesigned impellers.

Table 3.4. Comparison of redesigned impellers

	SYMBOL	UNIT	CHURCH	KOE
Blade Outlet Angle	β_2	^{0}	45.3	45.3
Blade Inlet Angle	β_1	^{0}	50.054	44.4
Inlet Diameter	D_{inlet}	mm	390	414
Blade Inlet Diameter	D_1	mm	398	408
Blade Outlet Diameter	D_2	mm	770	800
Blade Inlet Width	b_1	mm	99.193	162
Blade Outlet Width	b_2	mm	56.619	95

According to the updated results, when the impellers are compared, it is observed that there is a difference of 11% between the impeller inlet diameters, a loss of approximately 6% in the blade inlet diameters, a difference of 4% when the outer diameters of the impellers are analyzed, a value of 66% in the blade outlet widths and a change of 39% in the blade inlet angles. A value difference of 3% in the impeller diameters will not be observed when equations 3.86, 3.87, 3.88 are repeated according to the fan laws.

$$Q_{Church} = Q_{KOE} x \left(\frac{D_{Church}}{D_{KOE}}\right)^3 = 9.417x\left(\frac{0.770}{0.8}\right)^3 = 8.40\frac{m^3}{s} \Rightarrow \%10.76$$

$$P_{Church} = P_{KOE} x \left(\frac{D_{Church}}{D_{KOE}}\right)^2 = 4200x\left(\frac{0.770}{0.8}\right)^2 = 3892.95\ Pa \Rightarrow \%7.31$$

$$W_{Church} = W_{KOE} x \left(\frac{D_{Church}}{D_{KOE}}\right)^2 = 107x\left(\frac{0.770}{0.8}\right)^5 106.33\ kW \Rightarrow \%0.014$$

According to the obtained calculation results, there is no significant difference between the impeller geometries. In addition, these calculations are valid if it is accepted that the losses in the path from the entry of the flow into the fan to the impeller and from the impeller outlet until the fan discharges the fluid out of the volute are equal.

3.5.2. Comparison of the Volute

If we compare the volute designs: KOE prefers to keep the volume around the impeller wider and larger, but the calculation method proposed by Church results in a more compact and narrower volute geometry. In addition, due to the wide volute width, a conical throat is used at the inlet of the

KOE fan casing. Thanks to this throat, a wider cross-section is created at the body inlet compared to the impeller inlet, and with a slight expansion when entering the impeller, the fluid enters the impeller with some radial velocity. Since the Church's volute body is narrow, a channel with the same cross-section as the impeller inlet cross-section was created. For this reason, lower air velocities will occur in the channel at the body inlet of the KOE.

The technical drawing of the existing tested volute is given in Figure 3.14.

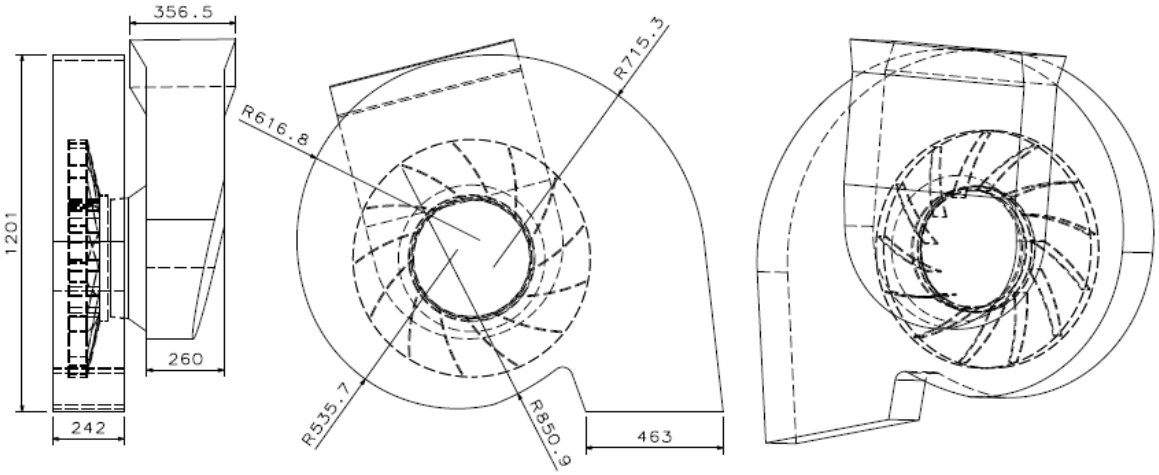


Figure 3.14. KOE snow ploughing fan

The technical drawing of the designed volute is given in Figure 3.15.

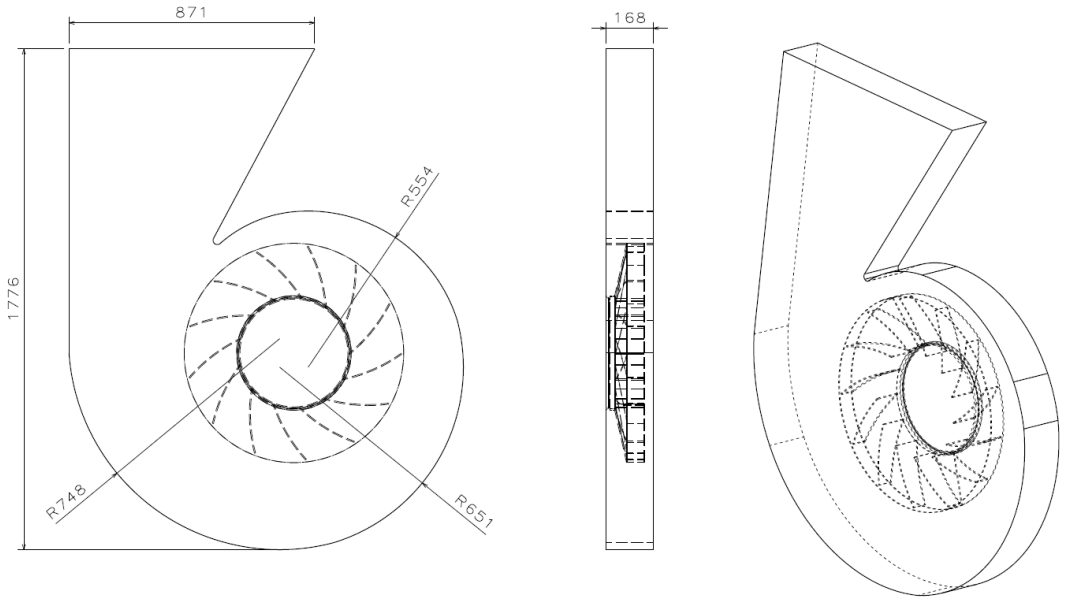


Figure 3.15. Designed volute 4-point method (Vibhakar,2015)

The biggest difference between volutes is in their width. The 4-point method design used in Vibhakar's (Vibhakar,2015) study is taken as an example. According to this study, the width of the volute is considerably narrower than the width of the existing fan. Also, in the designed fan, the

impeller is closer to the throat. This will increase the speed in the throat, which is the narrowest section. As the speed is high and the cross-section is narrow, the direction of the flow will be directed more into the volute and the losses are expected to be less. In the existing fan, the volute is wider and the impeller is farther away from the throat, so some of the flow will take the easy way out to the volute outlet.

3.5.3. Methodology

The centrifugal fan with backward tilted blades belonging to the Snow Plough and blowing vehicle at the KOE site was disassembled and compared with the technical drawings of the product. The product was verified with 2D technical drawing control and as a result, it was modeled in 3D through the Part Design, Sheet Metal Design and Surface design modules in CATIA V5 program. The 3D modeled fan was adapted into Ansys software.

In the Space Claim and Design Modeler modules in Ansys software, arrangements were made on the solid model to be suitable for flow analysis. Parts and assembly groups that have no effect on the flow and have the potential to reduce the performance of the analysis program have been removed. Since the fan of the relevant snow plough was designed in accordance with the production and the welded areas were not specified in the drawing program, the rough volume was obtained by creating a surface by taking sections of the relevant areas and solidifying them with the 'extrude' command. Afterwards, sheet materials, which are solid regions, were removed from the flow volumes with the 'interference' command. In accordance with the analysis environment, the flow volume in the fan was divided into three regions as impeller, fan inlet and outlet housing. With the 'Share Topology' command, the regions that are in contact with each other are determined, allowing the use of common nodes in these regions during structural meshing. The created geometry was checked with the 'Stitch, Gap, Missing Face and other Repair' commands in SpaceClaim and the regions with superficial topology errors were corrected. The created structure was transferred to the 'Design Modeler' program and the drawing phase was completed by defining 'Fluid' in all regions. Figure 3.16 shows an image of the impeller of the KOE snow plough with current values, prepared in space claim and prepared as a flow volume in design modeler.

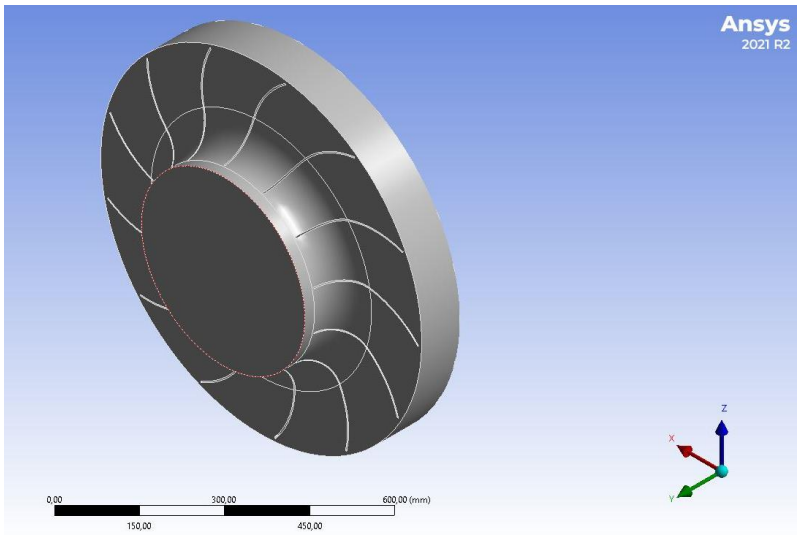


Figure 3.16. Volume flow of tested fan impeller

Figure 3.17 shows the flow volume rendered images of the volute and inlet sections of the tested existing fan. Figure 3.18 shows the cross-section of volume flow.

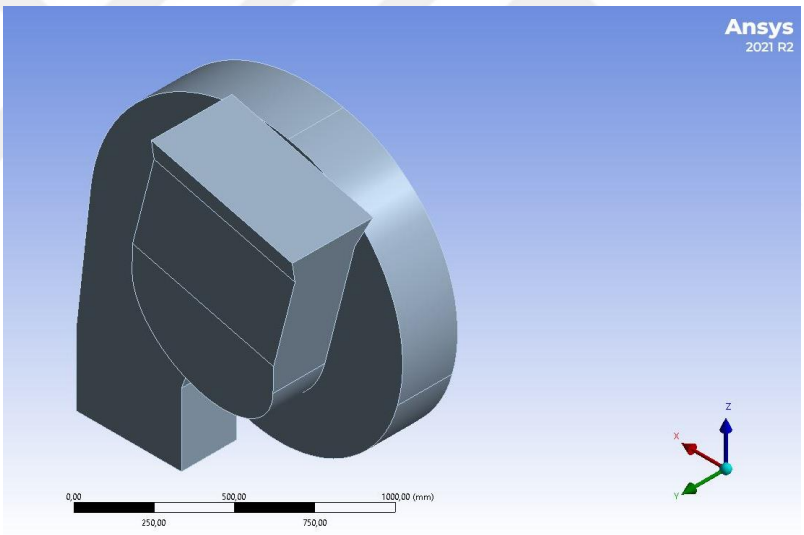


Figure 3.17. Volume flow of tested fan

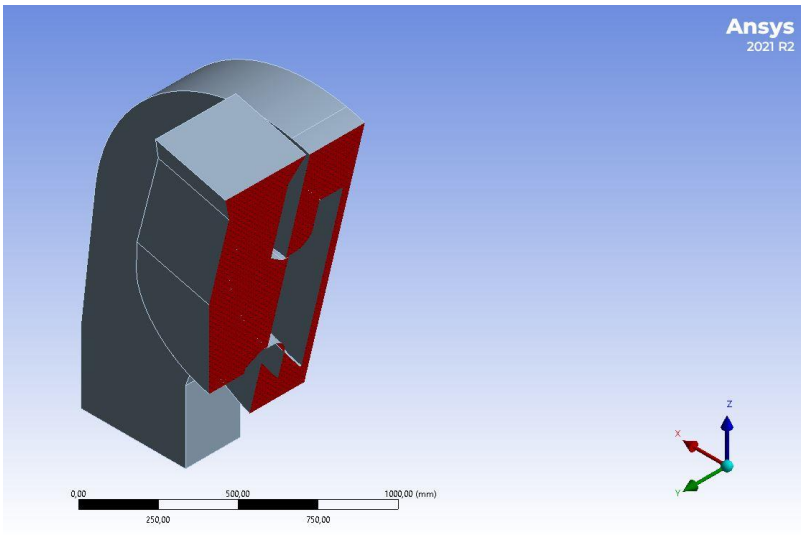


Figure 3.18. Volume flow of tested fan

As a result of adaptation, the model was transferred to the Meshing module in Ansys Workbench. In this program, which is a structural mesh modeling module, the created flow volume is divided into small geometric elements with known geometry and dimensions. Analysis programs enable these structural mesh elements to be solved by iteration of the relevant equations of fluid mechanics with different algorithms and to obtain results in the desired regions of the flow volume. Basically, mesh elements vary according to the type of analysis as 2-dimensional and 3-dimensional. Two-dimensional elements are triangle, quadrilateral and three-dimensional elements are tetrahedron, hexahedron, prism/wedge, pyramid and polyhedron. Figure 3.19 is shown the meshing type. (Ansys INC, 2017)

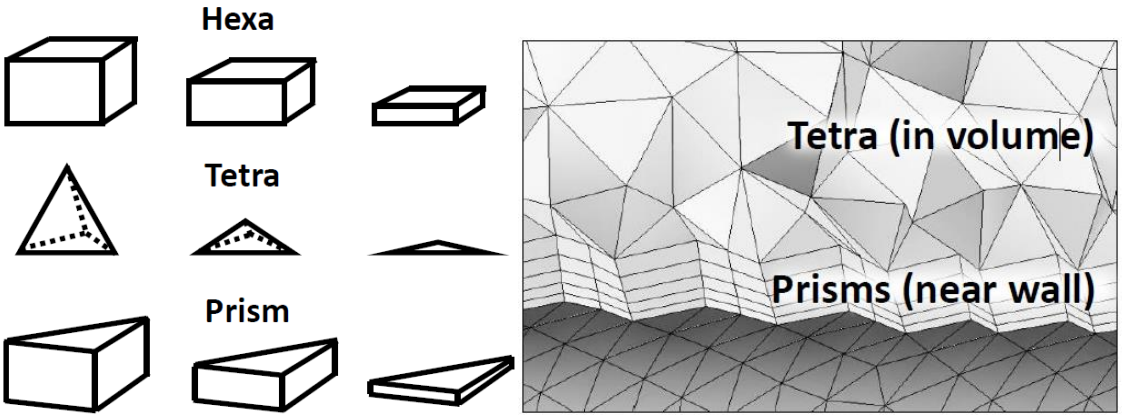


Figure 3.19. Meshing model (Ansys INC, 2017)

With the help of the 'Sizing' command in Meshing, corners, edges and surfaces can be divided into small geometries with the element size entered. With these arrangements, fine and coarse mesh elements can be used. The mesh elements created have quality values that are included in the program and accepted in the literature. 'Element Quality', 'Aspect Ratio', 'Skewness' are the most important of

these quality criteria and must be below certain values for the analysis to start. Skewness mesh metrics spectrum is shown in Table 3.5 **(Ansys INC, 2017)**. Figure 3.20 shows the meshing model of tested fan.

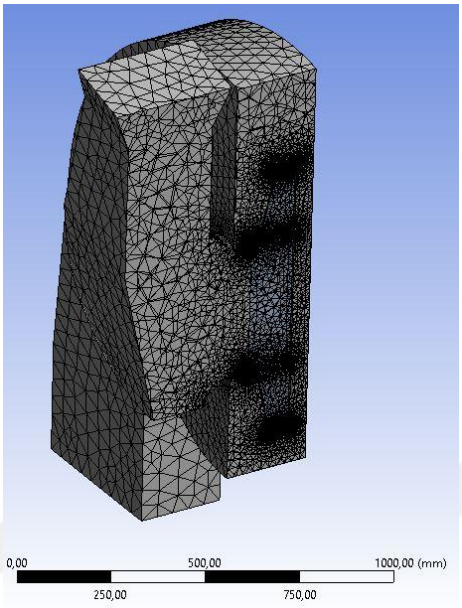


Figure 3.20. Meshing model of tested fan

Table 3.5. Skewness mesh metrics spectrum (Ansys INC, 2017)

Excellent	Very good	Good	Acceptable	Bad	Unacceptable
0-0.25	0.25-0.50	0.50-0.80	0.80-0.94	0.95-0.97	0.98-1.00

The tested fan skewness value is shown in Figure 3.21 and Table 3.6.

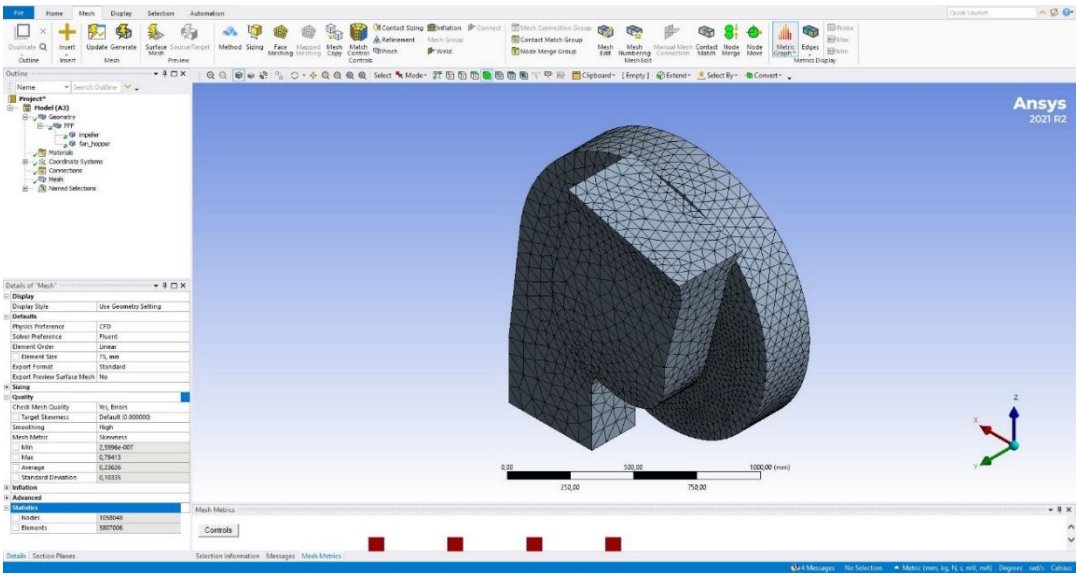


Figure 3.21. Skewness of the tested fan

Table 3.6. Skewness value of the tested fan

Min	Max	Average
2.5996e-007	0.79413	0.23626

Orthogonal Quality mesh metrics spectrum is shown Table 3.7 (Ansys INC, 2017).

Table 3.7. Orthogonal Quality mesh metrics spectrum (Ansys INC, 2017)

Unacceptable	Bad	Acceptable	Good	Very good	Excellent
0-0.001	0.001-0.14	0.15-0.2	0.20-0.69	0.70-0.95	0.95-1.00

The visual of the orthogonal quality data obtained after the mesh created by modeling the fan with data in KOE is shown in Figure 3.22. These values are reported numerically in Table 3.8.

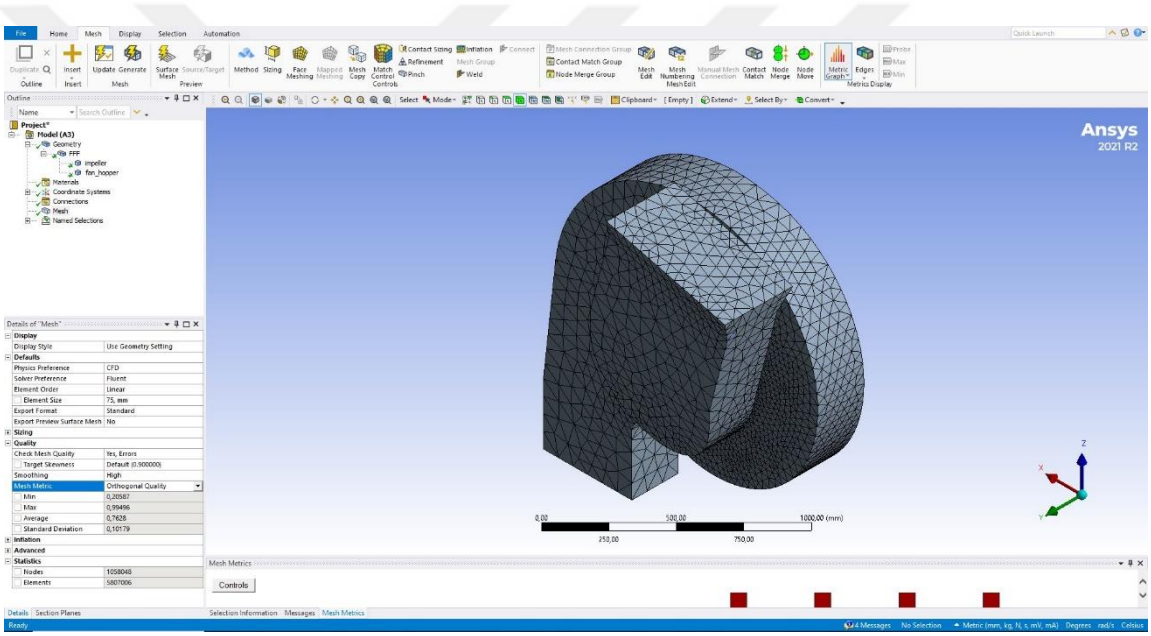


Figure 3.22. Orthogonal Quality of tested fan

Table 3.8. Orthogonal quality values of modeled tested fan

Min	Max	Average
0.20587	0.99496	0.7628

As a result of the experimental studies, a positive increase in these quality values (obtaining quality mesh) significantly increases the accuracy of the analysis results. The total number of meshes created within the scope of the analysis is 5807006. After the meshing process, the number of meshes and quality values are optimized. The regions to be defined as boundary conditions were named in the 'Named Selection' section.

In the next step, the geometric structure created in the 'Setup' and 'Solution' stages, along with the definition of the analysis environment conditions, solution algorithms and methods to be

used were selected. Since it is predicted that the flow in the fan will remain below Mach number 0.3, 'Pressure-Based' solver type was selected as the solver type. Steady was chosen as the solver time to ensure that the analysis is time independent and the results are obtained at a specific angular velocity value. The effect of gravity is neglected. 'k-epsilon, Realizable, Enhanced Wall Treatment' is selected as the turbulence model and flow separations at wall boundary conditions (blade surface and volute walls) are considered. 'Air' was selected as the fluid material. The impeller flow volume was created by defining 'Impeller' and the Multiple Reference Frame (MRF) method was used by defining 'Frame Motion' in the 'Cell Zone Condition' section. This method allows the rotating volumes in the flow volume to be defined as 'moving' and is recommended for Steady State conditions. Boundary conditions are defined as atmospheric conditions at the inlet and outlet (101.325 kPa atmospheric conditions). 'Coupled' was chosen as the solver algorithm to solve the velocity and momentum equations simultaneously to save time. 1000 iteration steps were entered and analyzed.

The computer specifications used in the analysis are given below.

Software: Ansys Fluent 2021 R2, CATIA V5
Operating System: Windows 10, 64 Bit
Computer hardware specifications used:
Processor: Intel(R) Xeon(R) CPU E5-1650 v4 @ 3.60GHz (12CPUs) ~3.6GHz
Installed memory 32.0 GB

$$\dot{m} = Q \times \rho \Rightarrow Q = \frac{\dot{m}}{\rho} \tag{3.89}$$

$$W = T \times \omega = T x \frac{\pi N}{30} \tag{3.90}$$

Bamberger and Carolus (2017) obtained seven correlations determining the geometric impeller parameters from aerodynamic optimization. Their objective was to maximize the total-to-static efficiency while precisely matching the targeted design points.

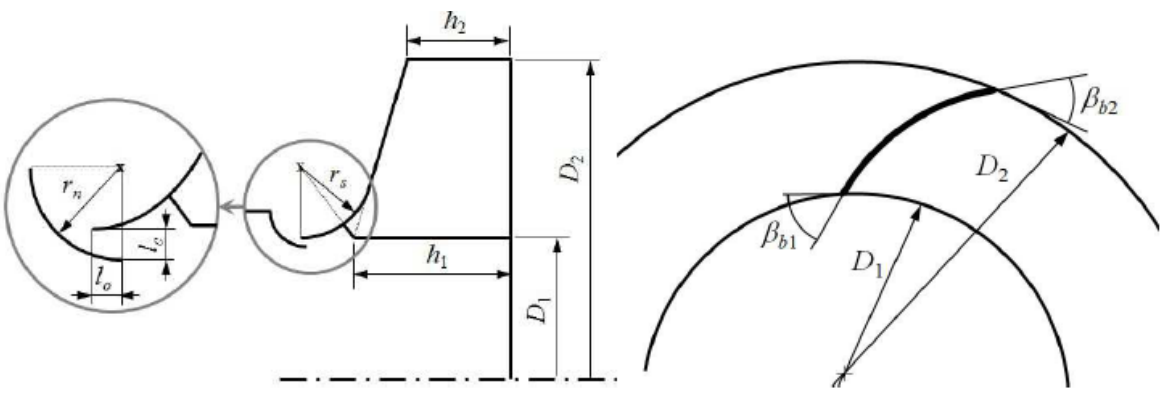


Figure 3.23. Geometrical parameters

Table 3.9. Independent geometrical parameters Bamberger and Carolus (2017)

Description	Symbol	Min. Value	Max. Value
Number of blades	Z	5	16
Diameter ratio	D_1/D_2	0.25	0.8
Inlet blade angle		20^0	60^0
Inlet blade width	h_1/D_2	0.025	0.4
Outlet blade width	h_2/D_2	0.025	0.4
Shroud radius	r_s/D_1	0.14	0.3

$$\text{Shroud radius} = \frac{r_s}{D_1} \rightarrow r_s = 0{,}22xD_1 \tag{3.91}$$

Table 3.10. Dependent and constant geometrical parameters Bamberger and Carolus (2017)

Description	Symbol	Min. Value
Nozzle radius	r_n/D_1	0.25
Clearance	l_c/D_1	0.02
Overlap	l_0/D_1	0.03

$$\text{Clearance} = \frac{l_c}{D_1} \rightarrow l_c = 0.02xD_1 \tag{3.92}$$

$$\text{Overlap} = \frac{l_0}{D_1} \rightarrow l_0 = 0.03xD_1 \tag{3.93}$$

$$\text{Nozzle radius} = \frac{r_n}{D_1} \rightarrow r_n = 0.25xD_1 \tag{3.94}$$



Figure 3.24. Exact geometry

3.5.4 Validation Methodology of exact Geometry

In order to verify analysis results data, the actual power consumption of the KOE fan was measured. Within the scope of this study, a fuel metering device was connected to the inlet line from the fuel tank and the return line of the fuel tank where the industrial type diesel engine that drives the fan is fed with fuel. Through this measuring device, the amount of fuel coming to the engine and the amount of fuel returning from the engine back to the fuel tank can be determined. The amount of fuel consumed by the engine can be determined. The main source of the power system of the snow plough and blower is an industrial type diesel engine. The diesel engine converts chemical energy into mechanical energy. There is a reducer directly connected to the diesel engine flywheel. The mechanical energy obtained is divided into 2 equal values through the gear reducer Figure 3.25.



Figure 3.25. Gear reducer

One axial piston hydraulic pump is installed at these two points. One of the hydraulic pumps is used to drive the fan and the other is used to drive the snow brush. System schematic is shown in Figure 3.26.

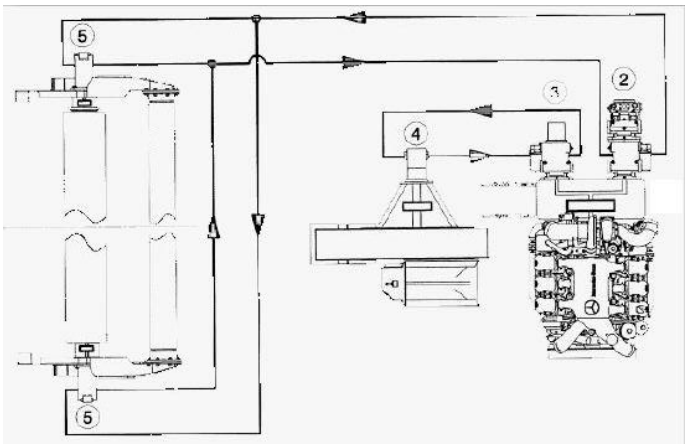


Figure 3.26. System schematic

The axial piston closed loop hydraulic pump converts mechanical energy into hydraulic energy by compressing and pressurizing the hydraulic oil that it sucks from the oil tank. A closed

loop hydraulic system means that the oil pumped by the pump is sent directly to the hydraulic motor and the return line of the motor is pumped directly to the return line of the hydraulic pump.



Figure 3.27. Closed loop hydraulic circuit

The converted hydraulic energy transfers power to the hydraulic motor used to turn the impeller of the fan through hydraulic fittings. The hydraulic motor mechanically transfers the hydraulic power it receives to the closed system rolling bearing to which it is connected via its own shaft through the key. The closed system bearing transfers the power it receives to the flange connected to the impeller of the fan through the key, thus ensuring the rotation of the rotor.

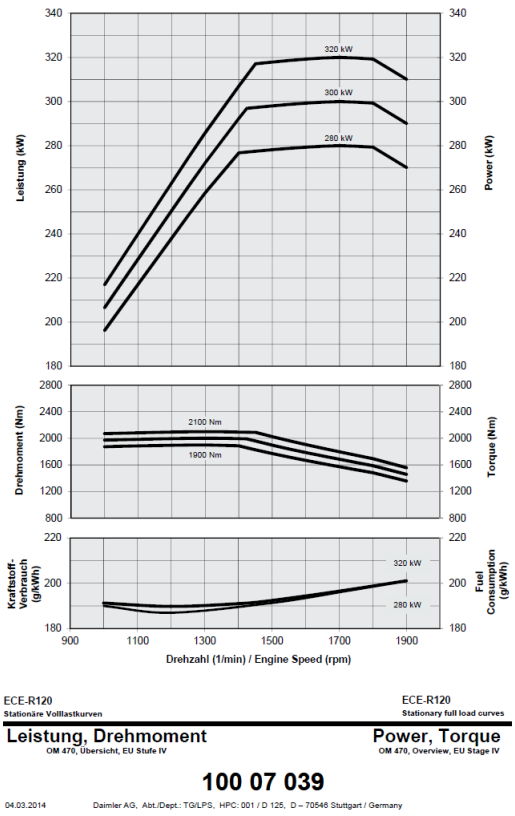


Figure 3.28. Engine performance curves (MTU, OM470)

$$N_{pump} = \frac{N_{engine}}{i_{gb}} \tag{3.95}$$

$$N_{pump} \text{ x } q_{pump} \text{ x } \eta_{hyd.} = N_{hyd.motor} \text{ x } q_{hyd.motor} \text{ x } \eta_{volumetric} \quad (3.96)$$

$$P_{pump} = (\Delta P x q_{pump})/(\eta_{mech.} x 60) \quad (3.97)$$

N_{pump}	: Hydraulic pump rotation	[rpm]
N_{engine}	: Diesel engine rotation	[rpm]
$N_{hyd.motor}$	: Hydraulic motor rotation	[rpm]
i_{gb}	: Transmission coefficient	
$\eta_{mech.motor}$	: Mechanical efficiency for hydraulic motor	[0,88]
$\eta_{hyd.pump}$	: Volumetric efficiency for hydraulic pump	[0,97] Hydraulic motor [0,96]
q_{pump}	: Hydraulic pump displacement	[cc, m^3]
$q_{hyd.motor}$	: Hydraulic motor displacement	[cc, m^3]
d_{hose}	: Diameter of hydraulic hoses	[mm]

Hydraulic hose diameter (d_{hose}) and hydraulic volumetric flow rate ($Q_{hydr.}$) are calculated theoretically with the following equations.

$$Q_{hydr.} = V_{hyd.pump} \text{ x } \eta_{hyd.} \text{ X } N_{pump} \quad \text{(Rexroth, Axial Variable Pump data sheet)} \quad (3.98)$$

$$d_{hose} = \sqrt{\frac{4Q_{hyd.}}{\pi x V_{hyd.} x 1000 x 60}} \quad \text{(Rexroth, Axial Variable Pump data sheet)} \quad (3.99)$$

4. RESULTS AND DISCUSSIONS

4.1 Tests and Validation

In the testing phase, the OM470 Stage IV diesel engine's rotation speed was set to N_{engine}: 1450 rpm, which is the speed at which it delivers maximum power, as determined by the power performance curve. According to the motor performance graph depicted in Figure 3.31, it is anticipated to consume 190 g/kWh of fuel at N_{engine}: 1450 rpm.

The gearbox attached to the engine increases this speed by 1.32 times, raising it to N_{pump}: 1880 rpm. Therefore, the rotational speed of the hydraulic pump is N: 1880 rpm. After the pump transfers power through hydraulic lines, when the speed of the hydraulic motor was checked with the digital tachometer device, it was measured as $N_{hyd.motor}$: 3246 rpm as shown in Figure 4.1. At the same time, the air velocities of the snow plowing and blowing machine were measured using a flow rate measurement device over a new channel, which is suitable for the blowing outlet and has measurement holes along the cross-section in the middle. The average value of these measurements was determined to be V_{ave}: 102.89 m/s.



Figure 4.1. Measurement with digital tachometer



Figure 4.2. Measurement of air velocity

From equation 3.95 revolution of Pump is calculated.

$$N_{pump} = \frac{1450}{0.758} = 1912.93 \text{ rpm} \Rightarrow \eta_{mech.} = \frac{N_{tested}}{N_{theor.}} = \frac{1880}{1912.93} = 0.98 = \%98$$

The revolution of hydraulic engine is defined by equation 3.96.

$$1880 \text{ x } 0.165 \text{ x } 0.97 = N_{hyd.motor} \text{ x } 0.09 \text{ x } 0.96 \Rightarrow N_{hyd.motor} = 3482.57 \text{ rpm}$$

When the test results are compared with the theoretical calculation, mechanical loss is experienced when the diesel engine transfers its power to the hydraulic pump and when the hydraulic engine transfers its power to the impeller.

$$\eta_{\text{mech.}} = \frac{N_{tested}}{N_{\text{theor.}}} = \frac{3246}{3482.57} = 0.93 = \%\ 93$$

After all connection and checks required for the entire testing procedure, a fuel consumption of 13991.25 grams was determined after half an hour of operation. When this value is divided by the value of 190 g/kWh obtained from the graph, it results in a fuel consumption of W: 143.5 kW. This value is higher by 25.44% from the data provided by the fan manufacturer and by 26.26% from the data obtained from the analysis. This result indicates that something is amiss in the system and needs to be checked.

Using equation 3.97 P_{pump} is reached. ΔP is defined by using P_{pump}.

$$\Delta P = \frac{P_{\text{pump}} x\ \eta_{\text{mech.}} x60}{q_{\text{pump}}} = \frac{143.5x0.88x60}{0.000165} = 236\ \text{bar}$$

When the changeable parameters affecting the power were examined, access to the hydraulic pump pressure was provided. The main factors that will affect the hydraulic pressure on the system are hydraulic hose diameter, sharp turns and hydraulic hose heads. In this respect, when the system was examined, it was observed that 3/4" inner diameter hose was used. Flow rate of hydraulic oil and diameter of the hoses are defined by equations 3.98 and 3.99 respectively.

$$Q_{\text{hydr.}} = 165ccx0.97x1880\ rpm = 300\ l/s$$

$$d_{\text{hose}} = \sqrt{\frac{4x300}{\pi x3x1000x60}} = 0.046\ \text{m} = 46\ \text{mm}$$

The flow rate of the hydraulic oil in the hose is selected between 2-5.5 m/s in the pressure line. In this calculation, V: 3 m/s is selected. According to the selected speed, the inner diameter of the hose should be 46 mm, while d_{hoses}: 19.05 mm hose was used in the system. It is a normal expected result that the pressure of the fluid increases in a narrow section. In addition, 90^0 hose heads were used on the hydraulic line. The hoses in the system were disassembled and the hose diameter was changed to d_{hoses}: 1 1/4". Hose fittings were also revised from 90^0 to 135^0. When the system was operated and the pressure between the hydraulic pump and the engine was measured with a pressure gauge, it was determined that it dropped to ΔP: 198 bar. With this change, ΔP: 38 bar loss in the

system was eliminated. When Equation 4.5 is recalculated, the power drawn by a W: 118.2 kW pump is obtained. While the initial control CFD a power consumption of 143.5 kW, the hydraulic pressure gain after the modification was W: 25.3 kW. According to the engine performance curve, the difference of W: 25.3 kW results in a fuel saving of 4807g/kWh in 1 hour of operation.

Table 4.1. Result differences of hydraulic hoses

Diameter of hose (inch)	¾”	1 ¼”
Power consumption (kW)	143.5	118.2
Hydraulic Pressure (bar)	236	198
Fuel consumption (g/kWh)	13991.25	9184.25

After conducting observations related to power and fuel consumption, the findings were transferred to the impeller geometry analysis environment designed of KOE fan. Adjustments were made in the designed geometry, followed by meshing. Similar values to those in the tested fan were obtained.

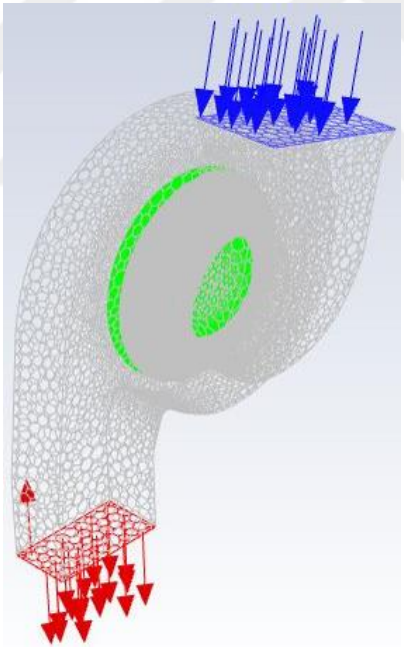


Figure 4.3. Meshing of KOE fan

Table 4.2. Skewness value of the KOE fan

Min	Max	Average
2.5996e-007	0.79413	0.23626

Table 4.3. Orthogonal Quality of KOE fan

Min	Max	Average
0.20587	0.99496	0.7628

After adjustment 1000 iteration steps were entered and analyzed. When the iterations were completed, it is seen that convergence has been completed successfully. According to the result of

the analysis, the speed of V_i= 79.078 m/s was determined at the impeller inlet. As a result of the test, this value transferred to us is V_i= 72.026 m/s. According to the result of the mass flow analysis, it is Q= 11.49 kg/s at the impeller inlet. When divided by the automatically assigned density value of ρ_{air}: 1.225 kg/m^3 in ANSYS, the volumetric flow rate is obtained. As a result of multiplying the obtained volumetric flow rate by 3600, a flow rate of Q= 33700 m^3/h is reached. The test value is Q= 33900 m^3/h. The analysis data shows the impeller inlet static pressure as ΔP= -4485.2319 Pa. In the test data, this value is stated as ΔP= -4200 Pa. The analysis data shows the impeller inlet static pressure as ΔP= -4485,2319 Pa. In the test data, this value is stated as ΔP= -4200 Pa. Again, according to the analysis results, the torque requirement data is T=315.7542 Nm. When we multiply the angular velocity by this torque value by using the equation 3.90, the power required for the wheel to rotate is obtained as W= 105.810 kW. The test data reported the required power as W=107 kW.

When the pressure contour is examined according to the analysis result of the tested fan, some pressure loss is observed in the directional area in the air inlet area of the impeller. A geometrical revision on the flow diversion will make the flow more pressurized. The pressure contour is shown in Figure 4.4.

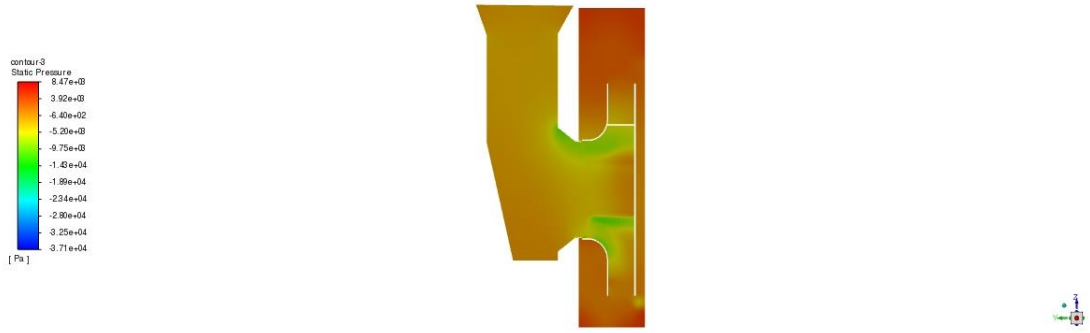


Figure 4.4. Pressure contour of tested fan

According to the analysis of the fan on the KOE, a dead zone has been identified in the inlet region of the fan. It can be presumed that the flow does not accelerate in the area that directs the air towards the blades when the air enters the fan, and the turbulent flow circulating in the directing region disturbs the quality of the flow by contacting the air entering the blades. It is considered that by narrowing the twisted manufacturing structure and manufacturing it with cylindrical bending, the flow can be brought into a more uniform form. Figure 4.5 shows the velocity contour of the tested fan.

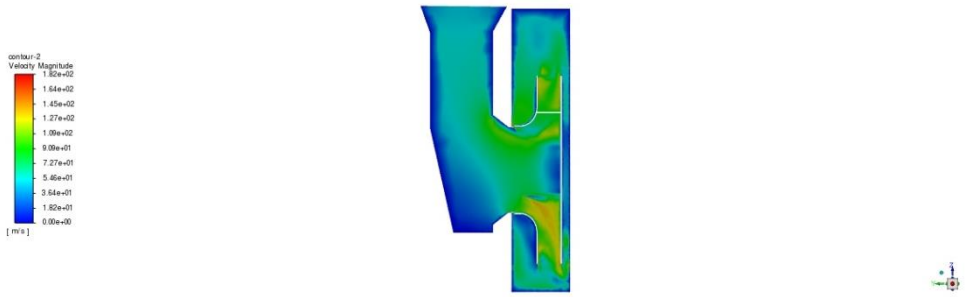


Figure 4.5. Velocity contour of tested fan

When examining the pressure contour at the inlet and outlet of the impeller, it is observed that the pressure at the outlet of the impeller is quite good. However, the same interpretation cannot be made for the inlet. Pressure loss has been observed in the lower edge section at the impeller inlet. This pressure loss is thought to be caused by the flow directed from the dead zone at the fan inlet.

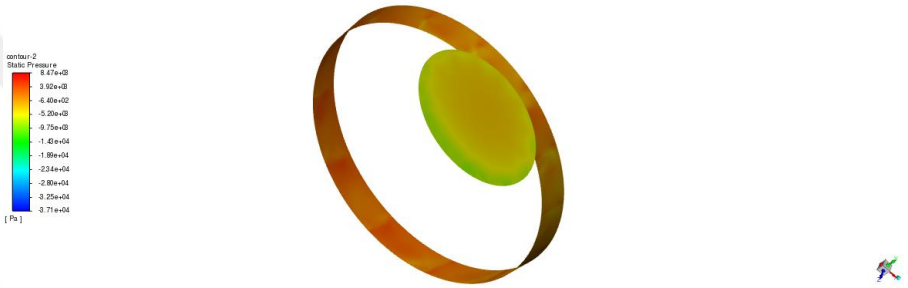


Figure 4.6. Pressure contour of the tested fan impeller

A comparison of the tested fan data with the analysis results is given in Table 4.4.

Table 4.4. Comparison of results between tested fan and analyzed tested fan

	Unit	Given values of KOE fan	Analyses Result of KOE fan	Test values of KOE fan
Impeller inlet suction Pressure	Pa	4200	4485.23	-
Impeller inlet Velocity	m/s	72,026	79.078	-
Volume Flow Rate	m^3/h	33900	33700	32506
Power Consumption	kW	107	105.81	118.2

4.2. Optimization by CFD

The fan impeller, developed according to the Church calculation, was analyzed using computational fluid dynamics (CFD) software with the same solution methods and environmental conditions, following the comparison of the test values of the current fan, existing data, and CFD analysis results. In Figure 4.7, as seen in the pressure contour of the impeller designed according to Church's method, the pressure distribution at the impeller inlet is more consistent compared to the

pressure distribution at the inlet of the snow plow vehicle's impeller. This consistency is thought to stem from the calculated impeller inlet diameter having a narrower structure.

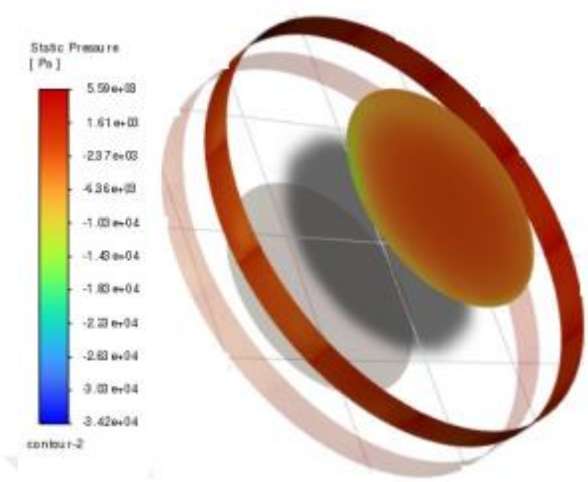


Figure 4.7. Pressure contour of Church design impeller

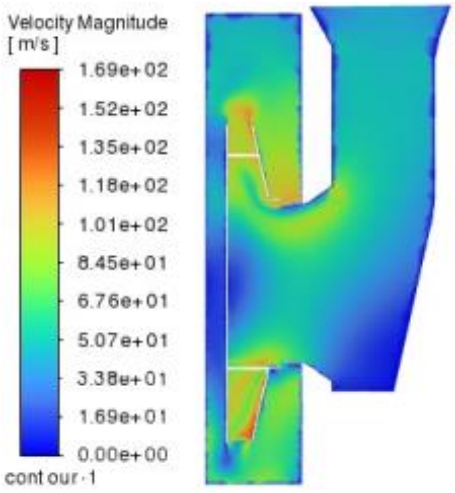


Figure 4.8.Velocity contour of Church design impeller

When examining the velocity contour, a dead zone has been identified once again at the inlet of the snow plow fan, where the flow occurs slowly. Additionally, due to the narrower geometry of the calculated Church fan impeller, it has been observed that the flow between the back surface of the impeller and the volute wall is almost negligible, as depicted in Figure 4.8.

Table 4.5. Comparison of the analyzed KOE fan and the impeller designed according to Church

	Unit	Analyses Result of KOE fan	Analyses Result of Church design
Impeller inlet suction Pressure	Pa	4485.23	4035
Impeller inlet Velocity	m/s	79.078	71.8
Volume Flow Rate	m^3/h	33700	30598
Power Consumption	kW	105.81	78.9

In subsequent studies, improvements were made using the impeller calculated according to Church.

4.2.1. Effect of blades on fan performance

The blade structure exerting the greatest impact on the flow was primarily examined within the scope of the conducted study. Due to the changes in the volute structure of the snow clearing and blowing device, which affects many components of the system, development efforts have been carried out specifically for the turbine. In this regard, the first change made was to match the

calculated Church turbine width to the existing volute structure. According to the Church calculation, a width of w=57mm was obtained, while the existing turbine had a width of w=80mm. As a result of the proportionality applied, the turbine width was determined to be w=113mm, and a CFD analysis was run under the same conditions. The result revealed a T= 19.8% decrease in the torque required to rotate the turbine and ΔP=2.7% decrease in inlet pressure. Additionally, this change resulted in Q= 8.5% decrease in mass flow rate. An efficiency increase of η= 6.9% was also achieved.

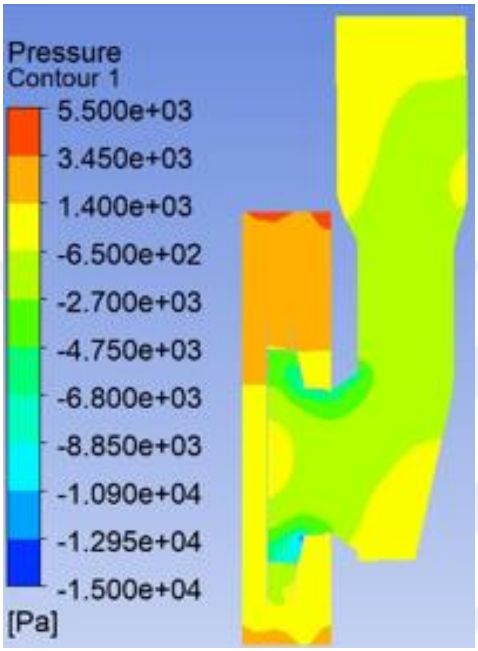


Figure 4.9. Pressure contour of the 57mm wide Impeller

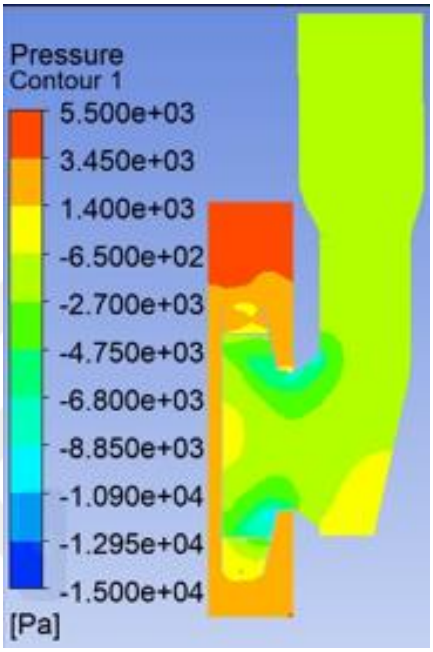


Figure 4.10. Pressure contour of the 113mm wide Impeller

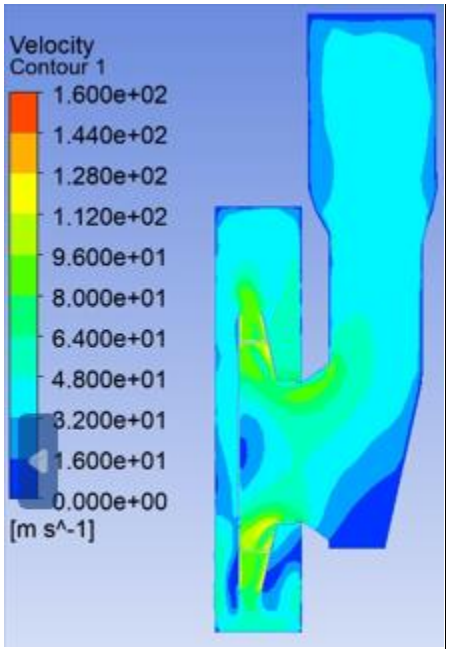


Figure 4.11. Velocity contour of the 57mm wide Impeller

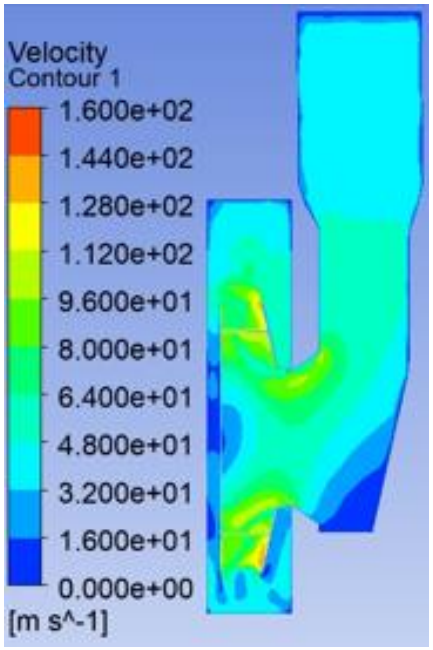


Figure 4.12. Velocity contour of the 113mm wide Impeller

Table 4.6. Comparison the width of Impeller by CFD results

Parameters	57mm Impeller width	113mm Impeller width	Rate
Torque (Nm)	187.831	260.459	+%38.7
Impeller inlet Pressure (Pa)	2902	4089	+%40.9
Volumetric flow rate (m^3/h)	26542.210	31254.42	+%17.7
Efficiency (η)	%41.6	%49.8	+%19.7

The data generated from calculations were revised with different numbers of blades, and each geometry was analyzed in the same CFD environment. Initially, a geometry with Z=9 blades was created. Subsequently, geometries with Z=11, Z=14, Z=15, and Z=17 blades were sequentially generated. These geometries were analyzed in the CFD environment. In the analysis evaluations, parameters such as inlet pressure, torque required to rotate the turbine, mass flow rate, and efficiency values were compared. It was observed that as the number of blades increased, the torque required to rotate the turbine also increased, while the inlet pressure and mass flow rate values also increased. However, the same cannot be said for the efficiency value. According to the analysis data of the Z=9-blade turbine, there is a T= 9.5% decrease in the required torque compared to the existing Z=13-blade turbine. Additionally, ΔP= 5.9% loss in inlet pressure is observed. While the volumetric flow rate decreases by Q= 3%, there is a η= 0.3% loss in efficiency. When the analysis data of the Z=15-blade turbine is compared with the existing Z=13-blade turbine, there is a T= 3.11% increase in the torque required to rotate the turbine. The resulting inlet pressure shows ΔP= 2.47% increase compared to the Z=13-blade turbine, and there is a Q= 1.14% gain in the flow rate. As a result of these data, it is observed that the efficiency increases by η= 0.51%. Upon examining the analysis data of the Z=17-blade turbine, it is observed that the increase in the required torque to rotate the turbine has a negative impact on efficiency due to its excessive nature. Therefore, the improvement efforts were subsequently continued based on the Z=15-blade turbine.

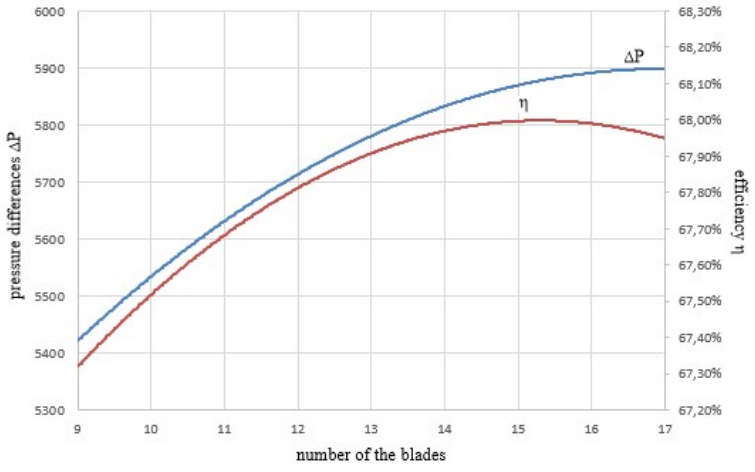


Figure 4.13. Relationship between the number of blades with pressure differences and efficiency

In the subsequent study, while keeping the turbine inlet diameter and width of the rotor constant, the outer diameter of the turbine was configured. The turbine diameter created according to the Church calculation was proportioned to the volute. A turbine model with a diameter of 840mm was created, and analysis was conducted on CFD with the same solution conditions. When compared to the results of the previous optimization, T= 21.32% increase in the torque required to rotate the turbine was observed. There is ΔP= 17.62% increase in turbine inlet pressure. While the mass flow rate increased by Q= 7.73%, the efficiency improved by η= 4.45%.

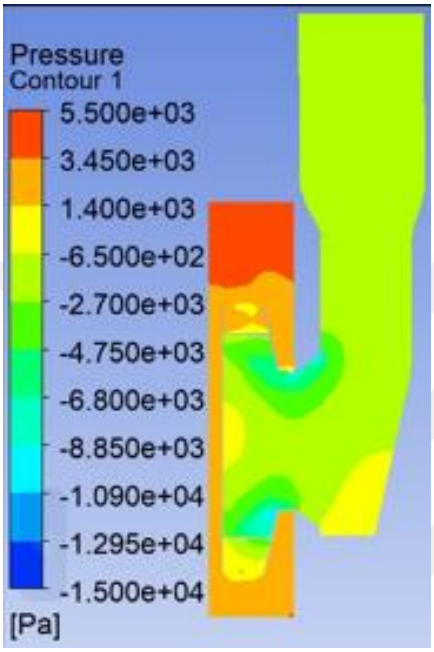


Figure 4.14Pressure contour of the 770mm diameter Impeller

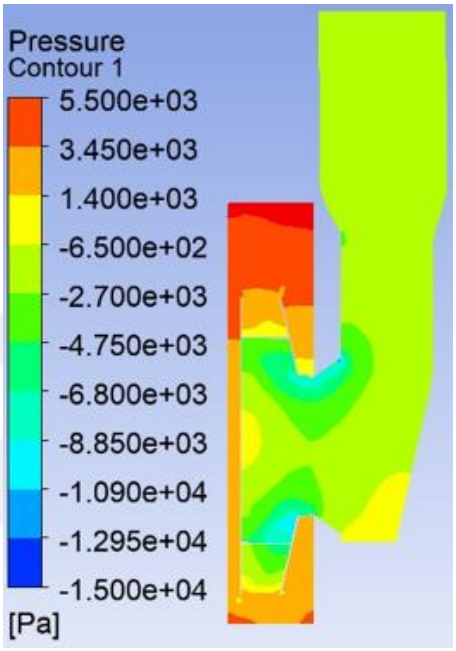


Figure 4.15. Pressure contour of the 840mm diameter Impeller

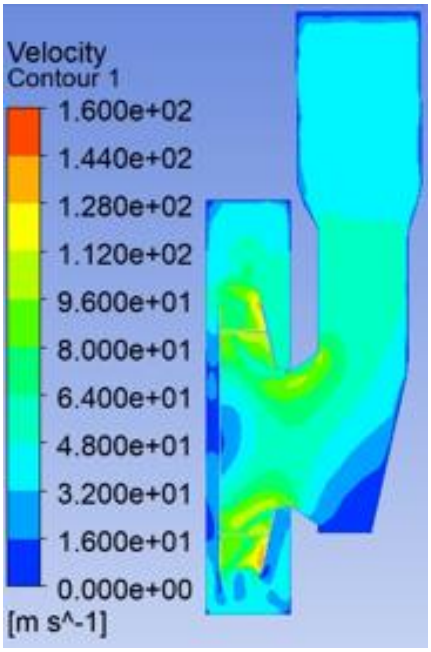


Figure 4.16. Velocity contour of the 770mm diameter Impeller

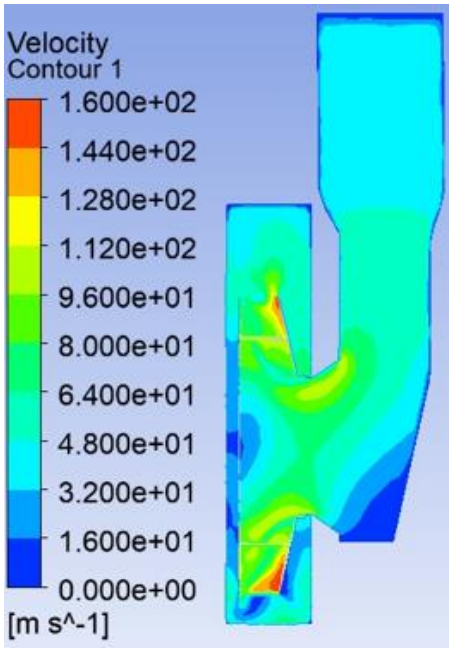


Figure 4.17. Velocity contour of the 840mm diameter Impeller

A separate study was conducted on the diameter at which the fluid enters the fan. Despite the determination of a ϕ_{inlet}= 25% increase in inlet diameter through calculation and the observation of η= 6.95% efficiency decrease according to the analysis data, there was T= 55.77% decrease in the torque required to rotate the turbine. However, due to the increase in the area of the inlet pressure, the turbine inlet pressure decreased by ΔP= 45.71%. Additionally, Q= 24.17% decrease in mass flow rate was observed. The step to optimize the shape was not evaluated positively due to the losses in mass flow rate and turbine inlet pressure.

During the comparison of the analysis data, it was observed that the fluid entering from the volute returned to the turbine inlet from the turbine outlet. This situation was considered to create losses. Following the example of the study by Bamberger and Carolus (2017), the turbine inlet was redesigned. With the designed turbine inlet geometry by using equations 3.91, 3.93 and 3.94 respectively, CFD analysis was conducted using the same solution methods. The obtained data were compared with Z= 15-blade, expanded, and enlarged Church turbine. According to the analysis results, there was T= 2.21% decrease in the torque required to rotate the turbine. While there was a significant increase of ΔP= 16.57% in turbine inlet pressure, the mass flow rate increased by Q= 3.38%. Despite the significant increase in turbine inlet pressure, the decrease in torque resulted in a significant efficiency increase of η: 23.24%.

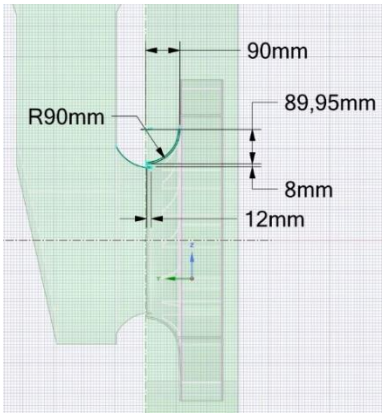


Figure 4.18. Geometry of Impeller redesigned Shroud Radius

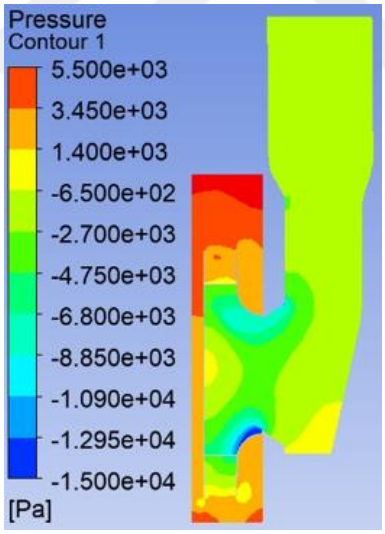


Figure 4.19. Pressure Contour of redesigned Shroud Radius

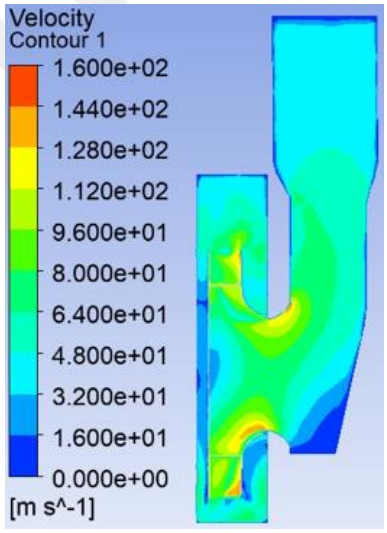


Figure 4. 20. Velocity Contour of redesigned Shroud Radius

In the scope of the Bamberger and Carolus (2017) study again, this time the geometry on the volute side was redesigned to redirect the flow into the turbine. The new design was defined by equation 3.95 and the new model is analyzed under the same CFD solution conditions. The new findings indicate T= 5.5% increase in torque, ϕ_{inlet}= 4.89% increase in turbine inlet diameter, Q= 6.99% increase in mass flow rate, and η= 6.37% increase in efficiency.

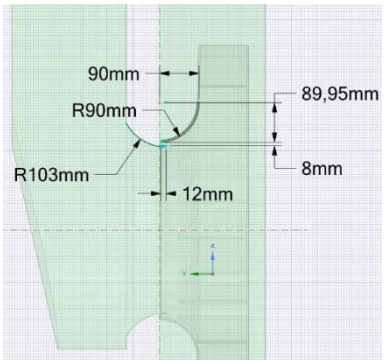


Figure 4.21. Redesigned geometry of the nozzle

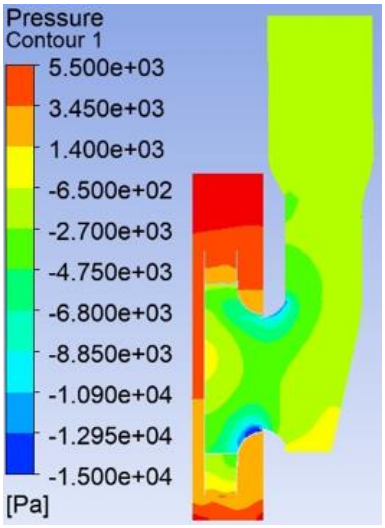


Figure 4. 22. Pressure Contour of the redesigned nozzle

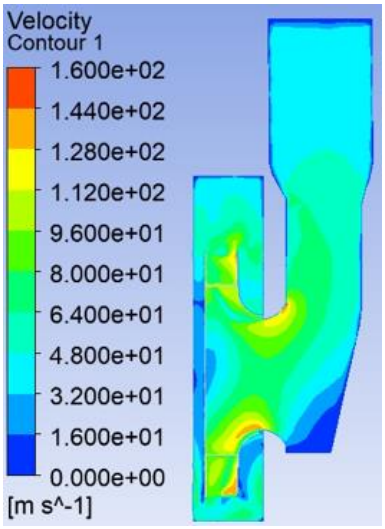


Figure 4.23. Velocity contour of the redesigned nozzle

4.2.2. Effect of blades angle on fan performance

In this study, the effect of three different blade angles on fan performance was compared in the analysis environment. Keeping all values constant according to the Church calculation, different blade exit angles ranging from $\beta_2 = 35^0$ to $\beta_2 = 55^0$ were entered and first checked on the calculation chart. A decrease in efficiency was observed at 35^0. It was observed that efficiency increased on the calculation chart from 35^0 to the existing blade angle of $\beta_2 = 45^0$. When the analysis was performed, it was confirmed that efficiency decreased at $\beta_2 = 35^0$. Continuing to increase the blade exit angle according to the calculation chart, it was observed that the change in fan performance efficiency was very small, and the turbine geometry was redesigned with a blade exit angle of $\beta_2 = 52^0$. The performance of the $\beta_2 = 52^0$ blade exit angle was evaluated under the same solution conditions. According to the analysis data, it was found that the torque required to rotate the turbine increased by T= 26.1%. The turbine inlet pressure increased by ΔP= 11.3%. When a mass flow rate comparison was made, there was Q= 5.5% increase. Taking all these data into account, the fan turbine performance efficiency decreased by η: 6,9%. It was observed that while the $\beta_2 = 52^0$ angled turbine was suitable when high flow rate and inlet pressure were important, there was a loss in efficiency when looked at from an efficiency perspective. Since a high torque requirement would lead to high energy and fuel consumption, the blade exit angle of the turbine was kept constant at $\beta_2 = 45^0$.

5. CONCLUSIONS AND RECOMMENDATIONS

Within the scope of the thesis study, a fan has been designed from scratch using a designated design method and updated using the CFD method. To assess the accuracy and precision of the CFD method, a fan used in airport blowers within the KOE product range with known values was selected, and the results obtained using the CFD method settings were compared with the static pressure at the design point. The results were found to be satisfactory with a margin of error of 6.39%. Mesh settings and qualities were used to create a mesh structure, and geometry was analyzed. The most suitable mesh settings were determined. During this period, to conduct validation, the vehicle's fuel consumption was tested. The presence of hydraulic losses in the system was identified, and improvement steps were implemented to prevent hydraulic pressure loss.

In the next stage, a rotor structure and volute were calculated according to the Church method. It was prepared for analysis and solved through the program. Positive results were obtained according to the analysis outcomes. When comparing the static pressure of the calculated impeller with the static pressure of the existing product, a deviation of $\Delta P = 3.92\%$ was observed.

In the scope of the improvement efforts, the most ideal number of blades has been determined to be $Z= 15$. An important relationship between the width of the volute and the turbine and the height of the volute and the turbine has been identified. With the updating of the turbine width according to the calculation, an efficiency gains of $\eta= 6.9\%$ has been achieved. As a result of increasing the turbine diameter according to the calculation, an additional $\eta= 4\%$ efficiency increase has been observed.

However, it has been observed that the most significant effect occurred as a result of the new designs made at the inlet of the turbine. When geometry was created only at the turbine inlet according to the calculation results, an additional $\eta= 18.9\%$ efficiency increase was achieved. While the turbine inlet pressure increased by $\Delta P= 14.2\%$, the required torque showed a decrease of $T= 2.3\%$, indicating a reduction in power consumption. Subsequently, with the redesign of the air guidance element in the volute corresponding to the turbine according to the calculation results, an additional $\eta= 6\%$ efficiency increase was achieved.

As a result, when the data of the existing fan geometry is compared with the data obtained from the improvement studies, the efficiency of the current fan, which was $\eta= 46.4\%$, has been increased to $\eta= 68\%$. The turbine inlet pressure has been improved from $\Delta P= 4200$ Pa to $\Delta P= 5881$ Pa. Initially, the mass flow rate, which was $Q= 33918$ m^3/s, has been increased to $Q= 37245$ m^3/s as a result of the studies. These improvements have been achieved with only $T= 10$ Nm increase.

Another study could be conducted on blade thickness. Reducing the thickness will decrease the torque value and lead to an increase in efficiency. Additionally, a separate study could be conducted on the material used in fan manufacturing.

REFERENCES

Amjadimanesh, A., Ajam, H. And Nezhad, A., H., 2015. Numerical Study of Blade Number Effect on the Performance of a 3D FC Centrifugal Fan. International Journal of Mechatronics, Electrical and Computer Technology, 5(15): 2109-2119

Aydın, Ü., 2020. Türkiye Enerji Görünümü. TMMOB, Ankara, 482p.

Balje, O., E., 1981. Turbomachines. John Wiley & Sons, New York, 514p.

Bamberger, K. and Carolus, T., 2017. A Novel Optimization Based Design Method for Centrifugal Fans. Proceedings of 12th European conference on Turbomachinery Fluid dynamics & Thermodynamics ETC12 , Stockholm, Sweden.

Behzadmehr, A., Mercadier, Y., Galanis, N., 2006. Centrifugal Fan using DOE Method and CFD Calculations. Journal Fluids Engineering, 128(3): 446-453.

Bleier, F., P., 1998. Fan Handbook. McGrawHill, Chicago, 397p.

Bruno, E., 1972. Design and Operation of Centrifugal, Axial-Flow and Cross Flow Fans. Pergamon Press, Oxford, 611p.

Bulgurcu, H., 2015. Havalandırma Tesisatı. TMMOB MİEM, İstanbul, 672p.

Ch, S., V., Anantharaman, K. and Rajasekaran, G., 2023. Effect of blade number on the performanca of centrifugal fan. materialstoday Proceedings, 72(3): 1143-1152.

Church, A., H., 1947. Centrifugal Pumps and Blowers. John Wiley & Sons, New York, 308p.

Çengel, Y., Boles, M., A., 1996. Mühendislik Yaklaşımıyla Termodinamik, Çeviren Derbentli, T.. McGrawHill, İstanbul, 867p.

Ding, H., Chang, T., and Lin, F., 2020. The Influence of the Blade outlet Angle on the Flow Field and Pressure Pulsation in a Centrifugal Fan. MDPI 8(11) : 14p.

Encyclopaedia Wikipedia : https://en.wikipedia.org/wiki/Fan_(machine) [last access date: 06.01.2024]

Enerdata : https://yearbook.enerdata.net/total-energy/world-consumption-statistics.html [last access date: 05.01.2024]

Hildebrandt, A. And Genrup, M., 2007. Numerical Investigation of the Effect of Different Back Sweep Angle and Exducer Width on the Impeller Outlet Flow Pattern of a Centrifugal Compressor With Vaneless.Diffuser. ASME Journal of Turbomachinery, 129(2): 421-433

Karanth, K.,V., and Sharma, N.,Y., 2010. Numerical analysis of a centrifugal fan for performance enhancement using boundary layer suction slots. Journal Mechanical Engineering Science, 224(8): 1665-1678.

Kearton, W., J., 1942. Influence of Number of Impeller Blades on the Pressure Generated in a Centrifugal Compressor and on its General Performance. Proceeding of the Institution of Mechanical Engineers 124(1): 481-568.

Kim, S., Park, J., Ahn, K., Baek, J., 2010. Improvement of the Performance of a Centrifugal Compressor by Modifying the Volute Inlet. ASME Journal of Fluids Engineering, 132(9): 7p.

Kovatz, A., Desmur., G., 1958. Pumps, Fans and Compressors. Blackie & Son Ltd, New York, 327p.

Lee, Y., Ahuja, V., and Hosangadi, A., 2011. Impeller Design of a Centrifugal Fan with Blade Optimization. International Journal of Rotationg Machinery, 2011 : 16p.

Meng, F., Dong, Q., Wang,Y., Wang,P. and Zhang, C., 2013. Numerical Optimization of Impeller for Backward-Curved Centrifugal Fan by Response Surface Methodology (RSM). Research Journal of Applied Sciences, Engineering and Technology, 6(13) : 2436-2442.

Myles, D., J., 1969. An Analysis of Impeller and Volute Losses in Centrifugal Fans. Proceeding of the Institution of Mechanical Engineers 184(1) : 253-277.

Onma, P., and Chantrasmi, T., 2017. Comparison of two methods to determine fan performance curves using computational fluid dynamics. 8th TSME-International Conference on Mechanical Engineering, Bangkok, Thailand.

Osborne, W., C., 1977. Fans. Pergamon Press, New York, 228p.

Rexroth:https://www.boschrexroth.com/en/us/media-details/53228c92-3f43-4af9-bbc5-e84e4d3dfd5 [last access date: 06.01.2024]

Rong, R., Cui, K., Li, Z. and Wu, Z., 2015. Numerical study of centrifugal fan with slots in blade surface 7th International Conference on Fluid Mechanics

Rong, R., Cui, K., Li, Z., Wu, Z., 2015. Numerical study of centrifugal fan with slots in blade surface Procedia Engineering 126(2015) : 588-591.

Shah, K., H., Vibhakar, N., N. and Channiwala, S., A., 2003. Unified Design and Comparatie Performance Evaluation of Forward and Backward Curved Radial Tipped Centrifugal Fan. Proceedings of the International conference on Mechanical Engineering 2003, Dhaka, Bangladesh.

Stepanoff, A., J., 1957. Radial und Axialpumpen. Springer, Berlin, 401p.

Stodola, A., 1945. Steam and Gas Turbines. Peter Smith Publications, New York, 1356p.

T.C. Enerji ve Tabii Kaynaklar Bakanlığı : https://enerji.gov.tr/bilgi-merkezi-enerji-elektrik [last access date: 07.01.2024]

Vibhakar, N., N., 2012. Studies on Radial Tipped Centrifugal Fan. Phd, South Gujarat University, Surat, 350p.

Yan, G., Dilin, P. And Lixiang, Z., 2010. Parameterized Design of Centrifugal Fan's Impeller. 2010 International conference on Measuring Technology and Mechatronics Automation Changsha, China.

CURRICULUM VITAE

Personal Information

Surname, Name : KOCA, Gökhan

Education

Degree	Institution	Graduation Year
Master's	Cukurova University	2024
Bachelor's	Cukurova University Mechanical Engineering Dep.	2012
High School	Ismail Sefa Özler Anatolian High School	2006

Work Experience

Year	Workplace	Title
2014-still	Koluman Automotive Industry	Sweeper Team Leader at R&D Department
2012-2012	Cukurova Silo Management	Production and Planning Engineer

Publications

1. Koluman’s Road Sweeper Centrifugal Fan Inlet Design, Mechanical Separation and Analysis
2. Turning Radius Calculation for Truck Mounted Sweeper Vehicles
3. Required Power and Torque Calculation for Hydraulically Driven Centrifugal Fans
4. Production Method of Throat Part in Centrifugal Fans
5. Prediction of Pressure-jump Coefficient of Sieve for Road and Runway Sweepers
6. Wx Resistance Calculation in Sub Frame Design of Sweeper Vehicles
7. Titreşim Sönümleme Takozlarının Seçimi ve Sönümleme Hesabı
8. Examining the Effects of Centrifugal Fan Body Design Changes on Air Flow Rate and Pressure Through Computational Fluid Dynamics
9. Numerical Study of a Blowing Vehicle’s Centrifugal Fan Flow Structures
10. Fan Impeller Optimization with Design Criteria

APPENDICES

APPENDIX A, TABLE 3.1					
Definition	**Symbol**	**Unit**	**1st Iteration**	**2nd Iteration**	**3rd Iteration**
Flow rate	Q	m^3/h	29700	30591.000	30591.000
Flow rate	Q	m^3/s	8.250	8.498	8.498
Diameter of duct	D_{duct}	mm	408	414.075	414.075
Diameter of duct	D_{duct}	m	0.408	0.414	0.414
Velocity of inlet duct (assuming)	V_{duct}	m/s	63.102	63.102	63.102
Density of air	ρ_{air}	kg/m^3	1.020	1.020	1.020
Mass flow rate	$\dot{m}$	kg/s	8.415	8.667	8.667
Density of air at atmospheric pressure	ρ_{atm}	kg/m^3	1.020	1.020	1.020
Atmospheric Pressure	P_{atm}	Pa	101325	101325.000	101325.000
Ideal gas constant	R	(N.m)/(mol.K)	287	287.000	287.000
Temperature of air at atmospheric pressure in C	T_{atm}	C	25	25.000	25.000
Temperature of air at atmospheric pressure in K	T_{atm}	K	298.150	298.150	298.150
Head	H	m	202.950	202.950	202.950
Gravity force	g	m/s^2	9.81	9.810	9.810
Velocity of inlet	V_{inlet}	m/s	63.102	63.102	63.102
Inlet pressure	P_{inlet}	Pa	99025.000	99025.000	99025.000
Atmospheric Pressure	P_{atm}	Pa	101325.000	101325.000	101325.000
Static Pressure (suction)	P_{static}	Pa	2300	2300.000	2300.000
Pressure ratio	ε_{pinlet}		0.9773	0.977	0.977
Temperature inlet	T_{inlet}	K	296.2189	296.219	296.219
Density of air at inlet	ρ_{inlet}	kg/m^3	1.1648	1.165	1.165
Flow rate inlet	Q_{inlet}	m^3/s	7.2244	7.441	7.441
Impeller inlet diameter	D_{inlet}	m	0.3818	0.387	0.387
Impeller blade inlet diameter	D_1	m	0.3894	0.395	0.395
The circumferential tangential velocity at the blade	u_1	m/s	65.2505	66.222	66.222
Rotation of impeller	N	rpm	3200	3200.000	3200.000
Blade radial inlet velocity	$V_1=V_{r1}$	m/s	66.257	66.222	66.222

APPENDIX A, TABLE 3.1					
Definition	**Symbol**	**Unit**	**1st Iteration**	**2nd Iteration**	**3rd Iteration**
From inlet velocity triangle	$\tan\beta_1$		1.015	1.001	1.001
Assumption: increase 3% for contraction of stream at inlet	β_1	^{0}	46.802	46.366	46.366
Impeller inlet relative velocity	v_1	m/s	92.993	93.677	93.677
Impeller blade area Assumption: Leakage loss %3	A_1	m^2	0.112	0.116	0.116
Blade inlet area thickness correction factor	$\acute{\varepsilon}_1$		0.942	0.942	0.942
Blade thickness	t	mm	4	4.000	4.000
Blade number	Z		13	13.000	13.000
Blade inlet width	b_1	mm	97.479	98.884	98.884
Pressure ratio impeller	ε_{pimp}		1.046	1.068	1.068
Impeller outlet pressure assuming equal to P_{atm}	P_2	Pa	103625.000	105722.337	105722.337
Adiabatic Head	H_{ad}	m	396.036	572.430	572.430
Constant	K'		0.58	0.580	0.580
Impeller outside diameter	D_2	m	0.488	0.587	0.587
Tangential velocity at the outlet of impeller	u_2	m/s	81.844	98.397	98.397
Radial outlet velocity	V_{r2}	m/s	56.319	56.319	56.319
Tangent outlet velocity vector	V_{u2}	m/s	26.112	42.665	42.665
Blade outlet angle	β_2	^{0}	45.3	45.300	45.300
Slip factor	W_z	m/s	14.059	16.902	16.902
Impeller inlet relative velocity with slip	W_{u2}	m/s	26.112	42.665	42.665
Outlet relative velocity with slip	W_2’	m/s	62.078	70.655	70.655
The loss tangential exit velocity	$V’_{u2}$	m/s	55.732	55.732	55.732
Absolute blade velocity with slip	$V’_2$	m/s	79.233	79.233	79.233
Absolute blade velocity	v_2	m/s	62.078	70.655	70.655
Angle between V_2'&V'_{u2}	$\alpha’_2$	^{0}	45.300	45.300	45.300
Theoretical head	$H_{theo.}$	m	368.749	462.787	462.787

APPENDIX A, TABLE 3.1					
Definition	**Symbol**	**Unit**	**1st Iteration**	**2nd Iteration**	**3rd Iteration**
Effective head	$H_{eff.}$	m	313.436	393.369	393.369
Impeller outlet pressure is based upon effective head	ε_{pimp}		1.037	1.046	1.046
Outlet pressure of impeller	P_2	Pa	102653.213	103593.520	103593.520
Impeller Pressure ratio	$\varepsilon_{pimp}^{0.283}$		1.013	1.019	1.019
Outlet temperature	T_2	K	300.050	301.756	301.756
Impeller outlet density	ρ_2	kg/m^3	1.192	1.196	1.196
Volumetric flow rate at the outlet	Q_{outlet}	m^3/s	7.271	7.463	7.463
Impeller outlet area	A_2	m^2	0.129	0.133	0.133
Outlet blade thickness factor	$\acute{\varepsilon}_2$		0.952	0.960	0.960
Blade exit height	b_2	mm	88.342	74.795	74.795
Leakage lose	Q_L	m^3/s	0.248	0.255	0.255
Suction pressure lose	$dP_{suction}$	Pa	1855.229	1855.229	1855.229
Suction pressure loss coefficient	k_i		0.800	0.800	0.800
Impeller pressure Lose	$dP_{impeller}$	Pa	111.324	61.737	61.737
Impeller pressure loss coefficient	k_{ii}		0.200	0.200	0.200
Disk friction lose	T_{df}	W	0.365	0.921	0.921
Material friction constant	f		0.005	0.005	0.005
Power loss due to disc friction	P_{df}	W	122.470	308.671	308.671
Hydraulic efficiency	$\eta_{hydr.}$		0.523	0.545	0.545
Volumetric efficiency	$\eta_{vol.}$		0.971	0.971	0.971
Total efficiency	η_{total}		0.508	0.530	0.530
Ideal shaft power	G	W	73705.903	70009.516	70009.516
Torque	T_{df}	Nm	251.371	238.765	238.765
Factor of safety	FOS		4	4.000	4.000
Volute base circle/inlet radius	R_2	mm	244.236	293.632	293.632
Radius of volute at angle 360º	R_3	m	0.174	0.209	0.209
Diameter of volute at angle 360º	D_3	m	0.348	0.418	0.418
Outlet velocity of Volute	V_4	m/s	55.811	39.635	39.635

APPENDIX A, TABLE 3.1					
Definition	**Symbol**	**Unit**	**1st Iteration**	**2nd Iteration**	**3rd Iteration**
Radius of volute tongue	R_t	mm	262.553	315.654	315.654
Volute tongue angle	θ_t	^{0}	4.103	4.103	4.103
Volute Pressure loss	$d_{Pvolute}$	Pa	130.783	375.123	375.123
Losing constant	k_{iii}		0.4	0.400	0.400
Height of Volute	H_v	m	0.547	0.658	0.658
Width of Volute	b_v	m	0.366	0.440	0.440
Exit volute area	A_v	m^2	0.130	0.188	0.188

APPENDIX A, TABLE 3.2					
Definition	**Symbol**	**Unit**	**1st Iteration**	**2nd Iteration**	**3rd Iteration**
Flow rate	Q	m^3/h	33900	34917.000	34917.000
Flow rate	Q	m^3/s	9.417	9.699	9.699
Diameter of duct	D_{duct}	mm	408	414.075	414.075
Diameter of duct	D_{duct}	m	0.408	0.414	0.414
Velocity of inlet duct (assuming)	V_{duct}	m/s	72.026	72.026	72.026
Density of air	ρ_{air}	kg/m^3	1.020	1.020	1.020
Mass flow rate	$\dot{m}$	kg/s	9.605	9.893	9.893
Density of air at atmospheric pressure	ρ_{atm}	kg/m^3	1.020	1.020	1.020
Atmospheric Pressure	P_{atm}	Pa	101325	101325.000	101325.000
Ideal gas constant	R	(N.m)/(mol.K)	287	287.000	287.000
Temperature of air at atmospheric pressure in C	T_{atm}	C	25	25.000	25.000
Temperature of air at atmospheric pressure in K	T_{atm}	K	298.150	298.150	298.150
Head	H	m	264.408	264.408	264.408
Gravity force	g	m/s^2	9.81	9.810	9.810
Velocity of inlet	V_{inlet}	m/s	72.026	72.026	72.026
Inlet pressure	P_{inlet}	Pa	97125.000	97125.000	97125.000
Atmospheric Pressure	P_{atm}	Pa	101325.000	101325.000	101325.000
Static Pressure (suction)	P_{static}	Pa	4200	4200.000	4200.000
Pressure ratio	ε_{pinlet}		0.9585	0.959	0.959
Temperature inlet	T_{inlet}	K	294.5993	294.599	294.599
Density of air at inlet	ρ_{inlet}	kg/m^3	1.1487	1.149	1.149
Flow rate inlet	Q_{inlet}	m^3/s	8.3614	8.612	8.612
Impeller inlet diameter	D_{inlet}	m	0.3845	0.390	0.390
Impeller blade inlet diameter	D_1	m	0.3921	0.398	0.398
The circumferential tangential velocity at the blade	u_1	m/s	65.7053	66.684	66.684

APPENDIX A, TABLE 3.2					
Definition	**Symbol**	**Unit**	**1st Iteration**	**2nd Iteration**	**3rd Iteration**
Rotation of impeller	N	rpm	3200	3200.000	3200.000
Blade radial inlet velocity	$V_1=V_{r1}$	m/s	75.627	75.627	75.627
From inlet velocity triangle	$\tan\beta_1$		1.151	1.134	1.134
Assumption: increase 3% for contraction of stream at inlet	β_1	^{0}	50.486	50.054	50.054
Impeller inlet relative velocity	v_1	m/s	100.183	100.827	100.827
Impeller blade area Assumption: Leakage loss %3	A_1	m^2	0.114	0.117	0.117
Blade inlet area thickness correction factor	$\acute{\varepsilon}_1$		0.945	0.946	0.946
Blade thickness	t	mm	4	4.000	4.000
Blade number	Z		13	13.000	13.000
Blade inlet width	b_1	mm	97.786	99.193	99.193
Pressure ratio impeller	ε_{pimp}		1.086	1.119	1.119
Impeller outlet pressure assuming equal to P_{atm}	P_2	Pa	105525.000	108688.877	108688.877
Adiabatic Head	H_{ad}	m	723.375	985.127	985.127
Constant	K'		0.58	0.580	0.580
Impeller outside diameter	D_2	m	0.660	0.770	0.770
Tangential velocity at the outlet of impeller	u_2	m/s	110.612	129.082	129.082
Radial outlet velocity	V_{r2}	m/s	64.283	64.283	64.283
Tangent outlet velocity vector	V_{u2}	m/s	46.999	65.469	65.469
Blade outlet angle	β_2	^{0}	45.3	45.300	45.300
Slip factor	W_z	m/s	19.000	22.173	22.173
Impeller inlet relative velocity with slip	W_{u2}	m/s	46.999	65.469	65.469
Outlet relative velocity with slip	W_2’	m/s	79.631	91.752	91.752
The loss tangential exit velocity	$V’_{u2}$	m/s	63.613	63.613	63.613
Absolute blade velocity with slip	$V’_2$	m/s	90.437	90.437	90.437

APPENDIX A, TABLE 3.2					
Definition	**Symbol**	**Unit**	**1st Iteration**	**2nd Iteration**	**3rd Iteration**
Absolute blade velocity	v_2	m/s	79.631	91.752	91.752
Angle between V_2'&V'_{u2}	α'_2	^{0}	45.300	45.300	45.300
Theoretical head	$H_{theo.}$	m	591.910	711.681	711.681
Effective head	$H_{eff.}$	m	503.123	604.929	604.929
Impeller outlet pressure is based upon effective head	ε_{pimp}		1.060	1.072	1.072
Outlet pressure of impeller	P_2	Pa	102914.368	104115.233	104115.233
Impeller Pressure ratio	$\varepsilon_{pimp}^{0.283}$		1.024	1.032	1.032
Outlet temperature	T_2	K	301.597	304.129	304.129
Impeller outlet density	ρ_2	kg/m^3	1.189	1.193	1.193
Volumetric flow rate at the outlet	Q_{outlet}	m^3/s	8.321	8.543	8.543
Impeller outlet area	A_2	m^2	0.129	0.133	0.133
Outlet blade thickness factor	$\acute{\varepsilon}_2$		0.965	0.970	0.970
Blade exit height	b_2	mm	64.694	56.619	56.619
Leakage lose	Q_L	m^3/s	0.283	0.291	0.291
Suction pressure lose	$dP_{suction}$	Pa	2383.699	2383.699	2383.699
Suction pressure loss coefficient	k_i		0.800	0.800	0.800
Impeller pressure Lose	$dP_{impeller}$	Pa	48.518	9.460	9.460
Impeller pressure loss coefficient	k_{ii}		0.200	0.200	0.200
Disk friction lose	T_{df}	W	1.644	3.569	3.569
Material friction constant	f		0.005	0.005	0.005
Power loss due to disc friction	P_{df}	W	550.772	1195.916	1195.916
Hydraulic efficiency	$\eta_{hydr.}$		0.570	0.637	0.637
Volumetric efficiency	$\eta_{vol.}$		0.971	0.971	0.971
Total efficiency	η_{total}		0.554	0.618	0.618
Ideal shaft power	G	W	129534.636	107695.205	107695.205
Torque	T_{df}	Nm	441.773	367.291	367.291
Factor of safety	FOS		4	4.000	4.000
Volute base circle/inlet radius	R_2	mm	330.083	385.202	385.202

APPENDIX A, TABLE 3.2					
Definition	**Symbol**	**Unit**	**1st Iteration**	**2nd Iteration**	**3rd Iteration**
Radius of volute at angle 360º	R_3	m	0.235	0.274	0.274
Diameter of volute at angle 360º	D_3	m	0.470	0.549	0.549
Outlet velocity of Volute	V_4	m/s	34.968	26.361	26.361
Radius of volute tongue	R_t	mm	354.840	414.092	414.092
Volute tongue angle	θ_t	^{0}	4.103	4.103	4.103
Volute Pressure loss	$d_{Pvolute}$	Pa	731.660	979.481	979.481
Losing constant	k_{iii}		0.4	0.400	0.400
Height of Volute	H_v	m	0.739	0.863	0.863
Width of Volute	b_v	m	0.495	0.578	0.578
Exit volute area	A_v	m^2	0.238	0.324	0.324